Yukon

YGS Miscellaneous Report 19

Assessment of the thermo-hydraulic properties of rock samples near Takhini Hot Springs and in the Tintina fault zone, Yukon

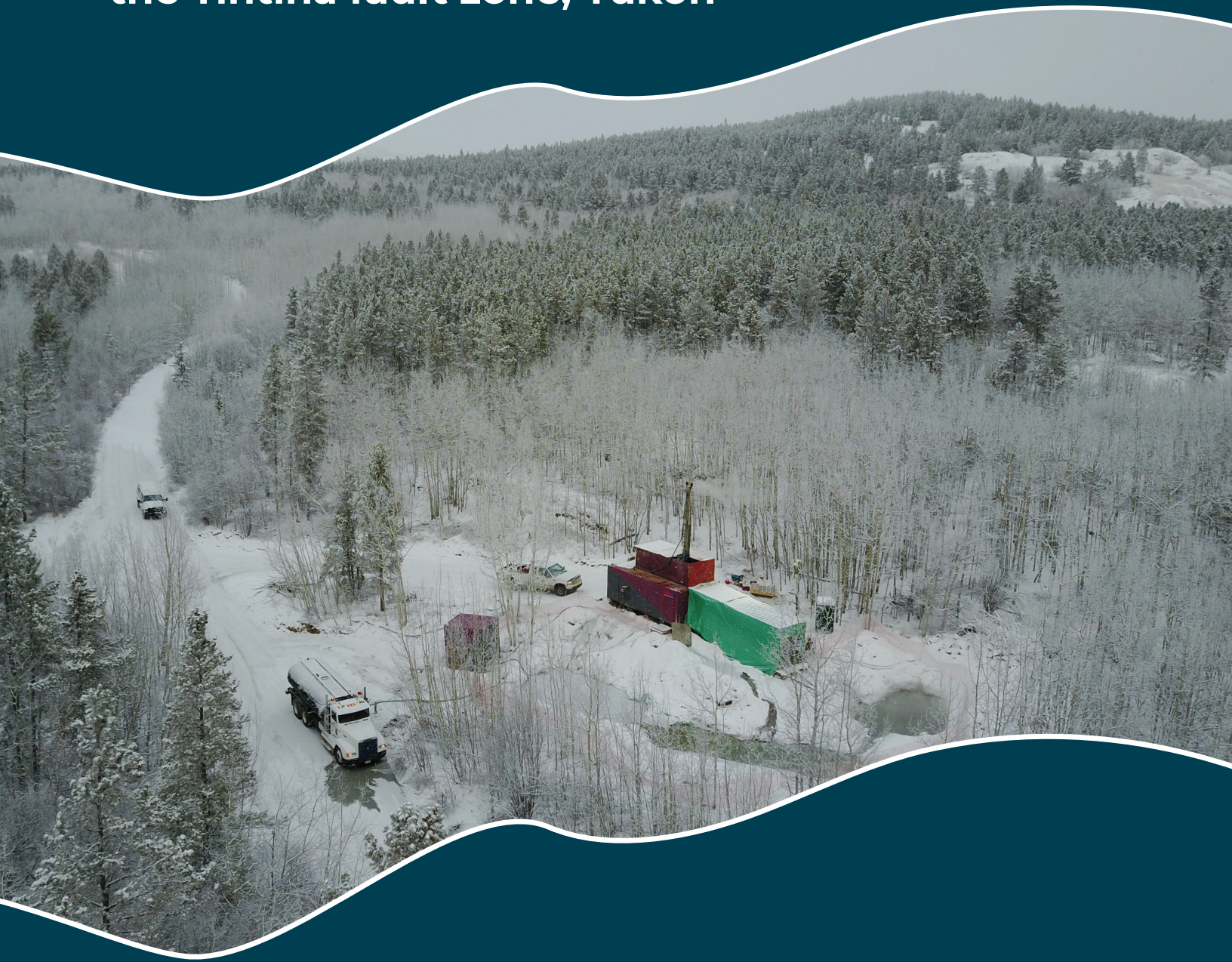

H. Langevin — Institut de la recherche scientifique, Québec
T.A. Fraser — Yukon Geological Survey
J. Raymond — Institut de la recherche scientifique, Québec

Published under the authority of the Department of Energy, Mines and Resources, Government of Yukon http://www.emr.gov.yk.ca.

Printed in Whitehorse, Yukon, 2020.

Publié avec l'autorisation du Ministères de l'Énergie, des Mines et des Ressources du gouvernement du Yukon, http://www.emr.gov.yk.ca.

Imprimé à Whitehorse (Yukon) en 2020.

This, and other Yukon Geological Survey publications, may be obtained from:
Yukon Geological Survey
102-300 Main Street
Box 2703 (K-102)
Whitehorse, Yukon, Canada Y1A 2C6
email geology@gov.yk.ca

Visit the Yukon Geological Survey website at http://data.geology.gov.yk.ca

In referring to this publication, please use the following citation:

Langevin, H., Fraser, T.A. and Raymond, J., 2020. Assessment of the thermo-hydraulic properties of rock samples near Takhini Hot Springs and in the Tintina fault zone, Yukon. Yukon Geological Survey, Miscellaneous Report 19, 30 p.

Cover photo: Geothermal drilling of the well at the Takhini drill site; located on Ta'an Kwächän Council Settlement Lands, 2 km from the Takhini Hot Springs.

Table of Contents

Abstract 1

Introduction 2

- Project background 2
- Geological setting 3
- Lithology 4

Methodology 5

- Sampling 5
- Thermal conductivity and diffusivity 8
- Relationship between thermal conductivity and temperature 9
- Radiogenic heat production 10
- Hydraulic conductivity 10
  - Consolidated rocks 10
  - Hydraulic conductivity of unconsolidated/brecciated rocks 11
  - Fractured rocks 11
- Takhini geological cross sections 12

Results 14

- Takhini area 14
  - Thermal properties in YGS-17-01 (well samples) 14
  - Thermal properties in outcrop samples 14
  - Hydraulic conductivity 17
  - Relationship between thermal conductivity and temperature of rocks 19
- Tintina well (YGS-18-01) 19
  - Thermal properties 19
  - Hydraulic conductivity 19
- Geological cross sections 22

Discussion 22

- Heat transfer and groundwater flow 22
  - Takhini well (YGS-17-01) 22
  - Tintina well (YGS-18-01) 24
- Geothermal setting 25
  - Takhini Hot Springs region 25
  - Tintina well region 26

Conclusions 26
Acknowledgements 28
References 28
Appendices 30

Abstract

As part of an emerging program to understand ground temperature and geothermal heat potential in Yukon, the Yukon Geological Survey drilled two temperature gradient wells in south-central Yukon: one near the Takhini Hot Springs in 2017, and a second in the Tintina Trench in 2018. This study presents the thermo-hydraulic properties of drill core from these wells and from selected outcrops, to evaluate heat transfer mechanisms in the subsurface and provide a heat flow model to characterize the geothermal potential of these regions. Thermo-hydraulic properties of the rocks in the Takhini well have a moderate thermal conductivity (average of ~3 W $m^{-1} K^{-1}$) and a low matrix hydraulic conductivity for consolidated rocks (on the order of 10^{-9} m s^{-1}), corresponding to a linear geothermal gradient of 16°C km^{-1} in the upper part of the well and suggesting conductive heat transfer between 50 and 450 m depth. Hydraulic conductivity of fractured and brecciated rocks on the order of 10^{-5} m s^{-1} (assuming a moderate fracture size of 100 µm), and topographic contrasts affecting the hydrostatic pressure driving groundwater flow in the area suggest that forced convective heat transfer in the bottom of the Takhini well is responsible for the strong geothermal gradient of 250°C km^{-1} observed between 450 and 500 m depth. The rocks in the Tintina well have low thermal conductivity (average of ~2 W $m^{-1} K^{-1}$) and hydraulic conductivity ranging from 10^{-5} to 10^{-3} m s^{-1}. The linear geothermal gradient (30°C km^{-1}) indicates conductive heat transfer even though the rocks are permeable. The proximity of the well to a mountain range suggests a shallow groundwater path in the Tintina well area, with no evidence of surface hot springs.

The location of steep faults appears to be a key pathway for deep groundwater to seep to surface and can explain the geothermal context near the Takhini well. Such a framework is a typical geothermal play type in orogenic belts. Although the Tintina well is found in a similar setting, this study does not identify potential for deep forced convective groundwater flow movements because hydraulic head difference along the faults may not be enough for the deep groundwater to rise since the faults are expected to be subvertical. This research, therefore, helps to characterize the subsurface and provides critical information needed for a successful exploration of geothermal energy resources.

Introduction

Project background

As part of the Yukon government's initiative to find green energy solutions, the Yukon Geological Survey (YGS) began a geothermal research program in 2016. Following regional assessments of geothermal potential, including mapping the depth to the Curie point (Witter and Miller, 2017), and calculation of radiogenic heat generative potential (Friend and Colpron, 2017), YGS drilled two 500 m temperature gradient (TG) wells to characterize the geothermal gradient in specific study locations. The first well, YGS-17-01, was drilled in the Takhini River area, northwest of the city of Whitehorse, ~2 km from a hot spring having a surface water temperature measuring 46°C. The well was drilled on land owned by the Ta'an Kwäch'än Council (TKC) First Nation, and the project was advanced in collaboration with the Da Daghay Development Corporation, the economic arm of the TKC. The second well, YGS-18-01, is located in southeastern Yukon, ~15 km southwest of the village of Ross River, in the crustal-scale, strike-slip Tintina fault zone (Fig. 1). This well was drilled on a section of the highway right-of-way on the South Canol road, in the traditional territory of the Kaska Dena Nation, in partnership with the Ross River Dena Council and the Dena Nezziddi Development Corporation. Drilling program details and results are summarized in Fraser *et al*. (2018). Stabilized downhole temperature was measured in the Takhini well at intervals of 50 m. This well has a variable geothermal gradient with depth (Fig. 2a): 16.5°C km^{-1} is found in the upper 450 m of the well while 250°C km^{-1} is present at the bottom 50 m (Fraser *et al*., 2018). In the Tintina well, stabilized downhole temperatures were measured at intervals of 20 m indicating an equilibrium geothermal gradient of ~31°C km^{-1} (Fig. 2b).

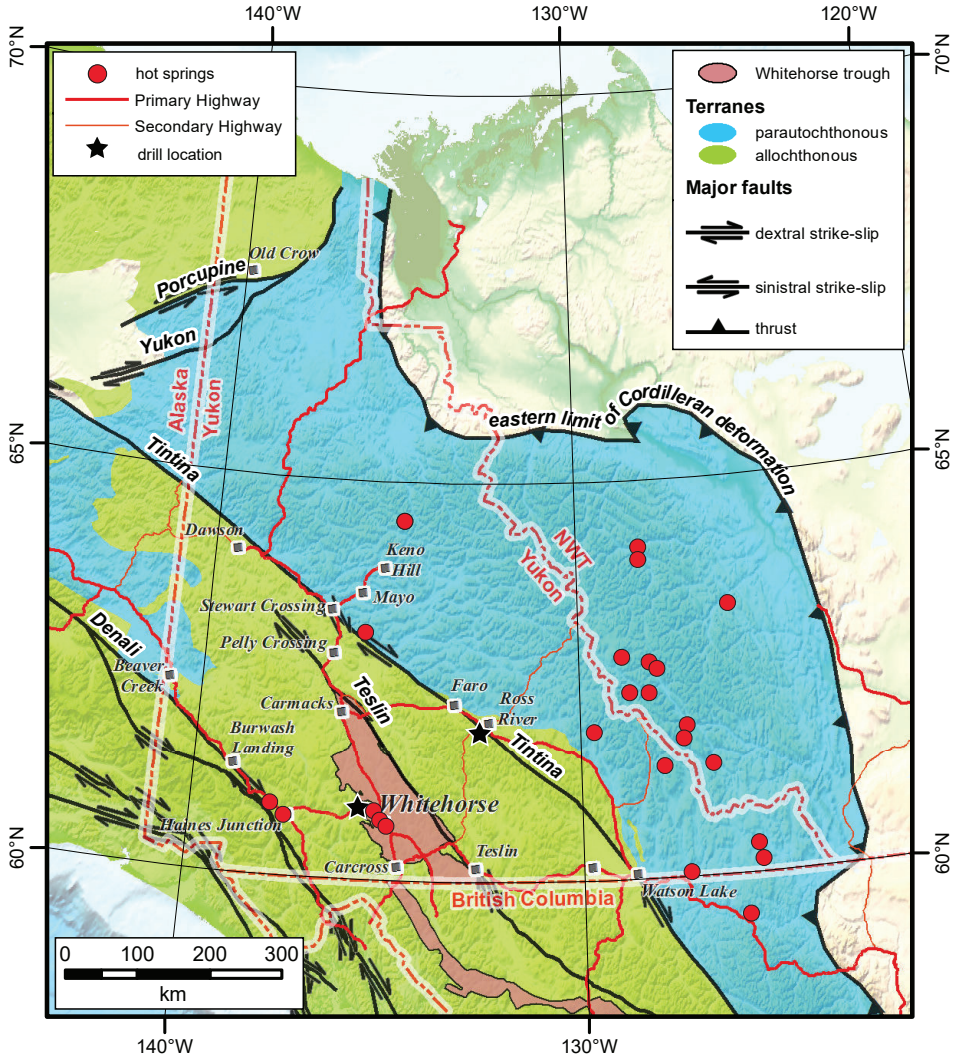

Figure 1. *Simplified terrane map of Yukon illustrating locations of major faults, hot springs, and the Whitehorse trough (Fraser et al., 2018).*

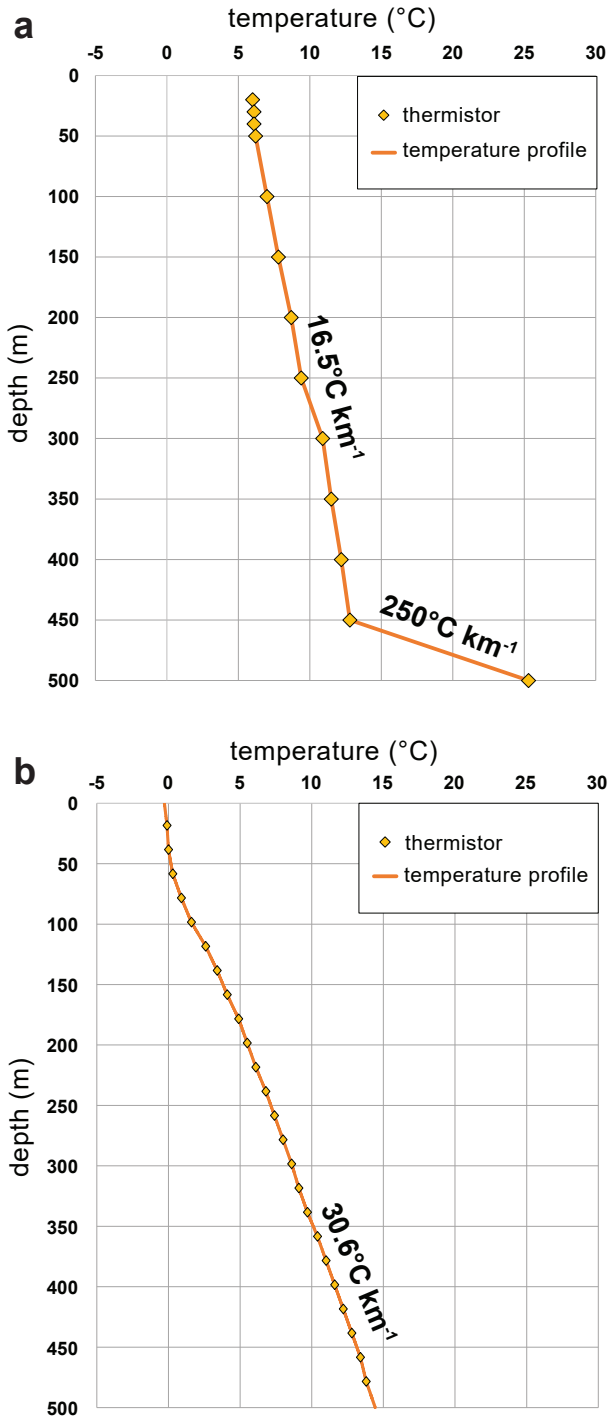

Figure 2. *Downhole temperature data and calculated geothermal gradient in the* ***(a)*** *Takhini well (YS-17-01) and* ***(b)*** *Tintina well (YGS-18-01; after Fraser et al., 2018).*

YGS and Institut national de la recherche scientifique (INRS) initiated a collaboration in 2019 to analyze rock samples from the YGS' geothermal research program at the Laboratoire ouverte de géothermie (LOG), in Québec. This paper reports on the findings of this collaboration. The study investigates heat transfer mechanisms present in YGS' temperature gradient wells in order to provide a better understanding of the geothermal potential of these regions. Data collection involved analysis of rock thermal and hydraulic properties on core samples, as well as on outcrop samples in the Takhini region. This study provides quantitative measures of thermal conductivity and diffusivity, radiogenic heat production and hydraulic conductivity values of the rock samples analyzed.

Geological setting

Yukon, in northwestern Canada, comprises rocks of the North American Cordillera, which record more than 1.8 b.y. of Earth history and the evolution of western North America (Nelson *et al.*, 2013). Two main geological domains occur in Yukon (Fig. 1): 1) Proterozoic to Triassic platformal and basinal sedimentary strata deposited on the North American continental margin to the northeast (parautochthonous terrane); and 2) Late Paleozoic and younger allochthonous island arc and ocean terranes that accreted to the North American margin, to the southwest, beginning in the Late Paleozoic. In Yukon, the dividing line between the two domains is for the most part the Tintina fault, a dextral strike-slip fault that has ~430 km of early Cenozoic displacement (Gabrielse *et al.*, 2006). Near Ross River and the location of the Tintina well, the fault zone is ~10 km wide and consists of six prominent subparallel fault strands linked by a series of high-angle synthetic faults (Mira Geoscience, 2017; Yukon Geological Survey, 2018a).

The Takhini well was drilled in sedimentary rocks of the Whitehorse trough (Fig. 3), an elongated northwest-trending Mesozoic sedimentary basin that extends 650 km from northern British Columbia to central Yukon (Fig. 1; Colpron *et al.*, 2015). In the vicinity of the well, Jurassic sedimentary rocks lie unconformably upon Upper Triassic marine sedimentary, volcanic and volcaniclastic rocks (Hart, 1997) and unconformably below Upper Jurassic to Cretaceous non-marine conglomerate and sandstone deposited in intermontane settings (Long, 2015). Middle Jurassic to Paleogene granitoid plutons intruded Whitehorse trough and older strata, including an Eocene granitoid pluton ~2 km west of the drill site (Hart, 1997; Yukon Geological Survey, 2018a).

Based on desktop studies (*e.g.*, depth to Curie point mapping; radiogenic heat potential from granite; *see* Fraser *et al.*, 2018) and its proximity to the 'Pacific Ring of Fire', the southwestern part of Yukon is expected to have the highest geothermal heat potential. Hot springs occur in various locations in the territory, although exclusively south of 65°N (Fig. 1).

Lithology

The Takhini well was drilled in the Richthofen formation and Nordenskiöld facies of the Whitehorse trough sedimentary basin (Fig. 3). Twelve distinct lithological units were encountered (Fig. 4), which are fully described in Langevin *et al.* (2020). Highly fractured intervals indicated by unconsolidated/brecciated rock occur between ~290 and 350 m depth. Felsic, intermediate and mafic dikes crosscut basinal or volcaniclastic sedimentary rocks.

Outcrops examined in the vicinity of the Takhini well include Carboniferous to Paleocene rocks: 1) variably deformed greenstone of the Mississippian (or older) Takhini assemblage; 2) Upper Triassic volcanic and sedimentary rocks of the Lewes River Group, including

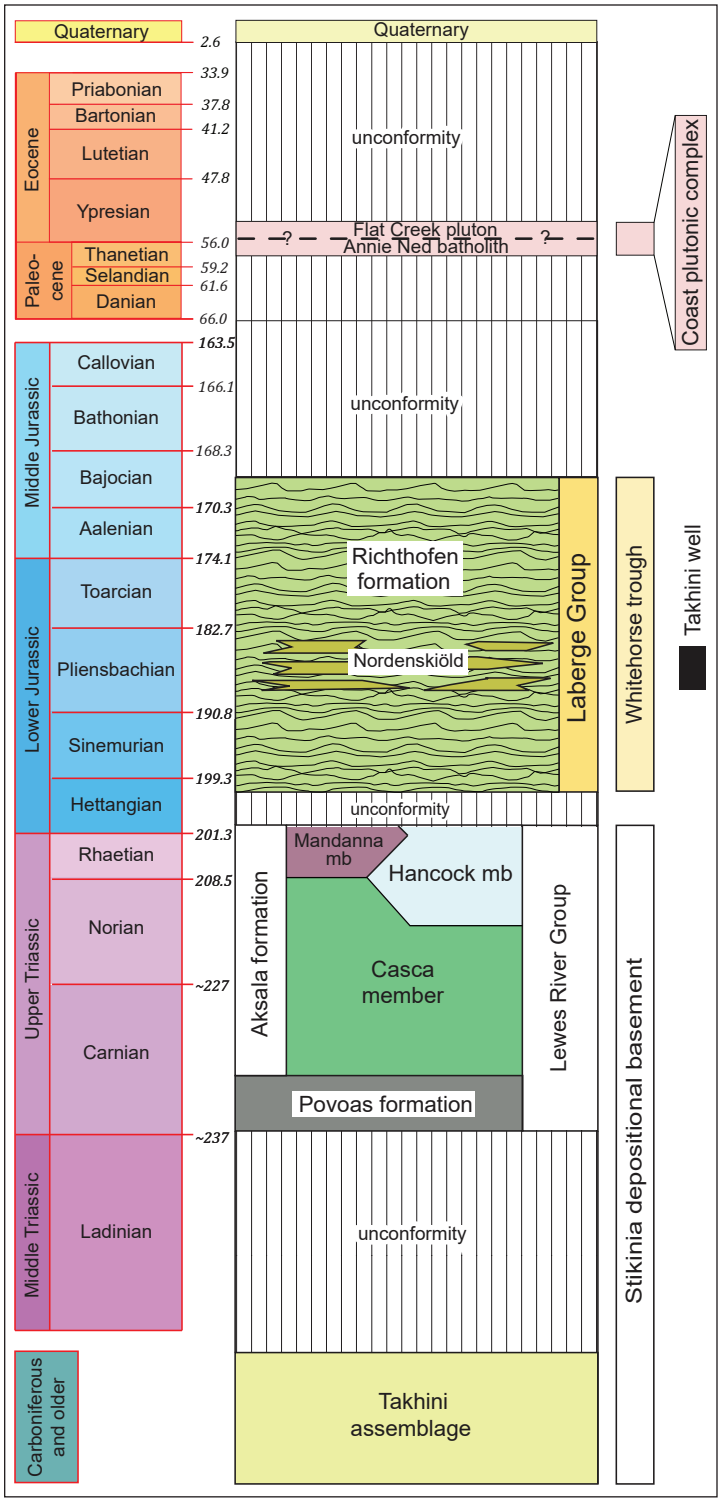

Figure 3. *Geological units in the Takhini well area (modified from Colpron et al., 2015).*

basalt of the Povoas formation, and volcaniclastic sandstone (Casca member), limestone/marble (Hancock member), and maroon sandstone and shale (Mandanna member) of the Aksala formation; and 3) clastic sedimentary rocks of the Laberge Group, including shale and sandstone of the Richthofen formation and minor volcaniclastic rocks of the Nordenskiöld facies. Paleocene intrusive rocks include granite and granodiorite of the Flat Creek pluton and Annie Ned batholith (Hart, 1997; Ruby Range suite of Colpron *et al.*, 2016).

Six sedimentary units were encountered in the Tintina well, ranging from clay to pebble/cobble conglomerate (Fig. 5). General lithological descriptions are provided in Fraser *et al*. (2018). As the well was drilled in a major fault zone, the core is overall poorly consolidated and rocks are difficult to assign to any formation or age (Fig. 6).

Methodology

Sampling

The primary focus for this study was the Takhini well and nearby outcrops. Forty-one core samples were collected from depths between 55 and 500 m, and represent all 12 lithological units encountered in the well (Fig. 4). An additional 41 outcrop samples from near the well supplement the sample set (Fig. 7). This additional sampling was undertaken to improve understanding of the distribution of the thermal and hydraulic properties in the region and at depth, and to characterize additional geological units not intercepted in the well that may affect regional groundwater flow and hot springs generation. A secondary focus was given to 11 samples collected from the Tintina well to provide thermal and hydraulic properties required for future heat flow assessments (Fig. 5).

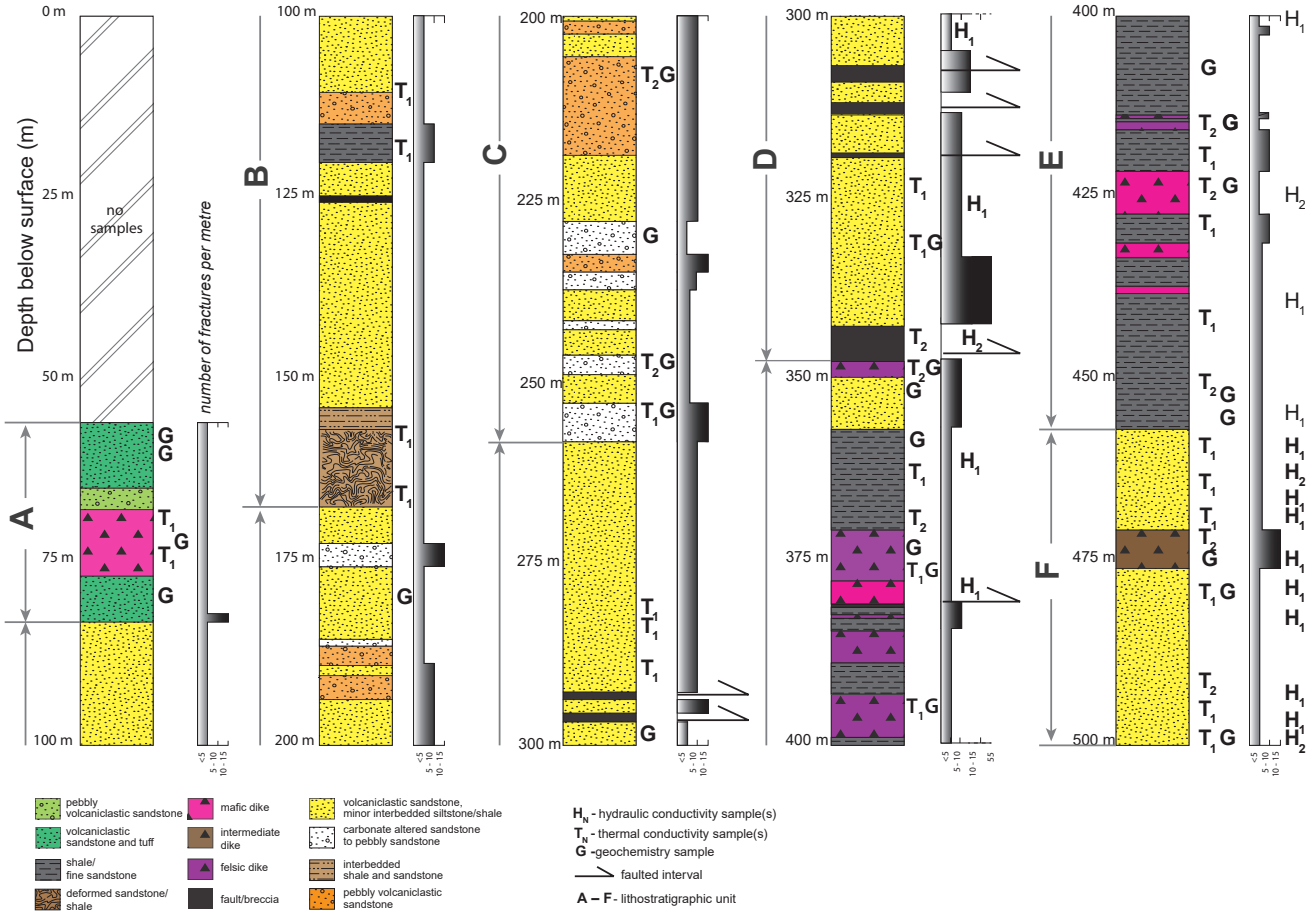

Figure 4. *Lithostratigraphy of the Takhini well (YGS-17-01) including fracture density, and locations of samples for thermal and hydraulic conductivity measurements and lithogeochemistry.*

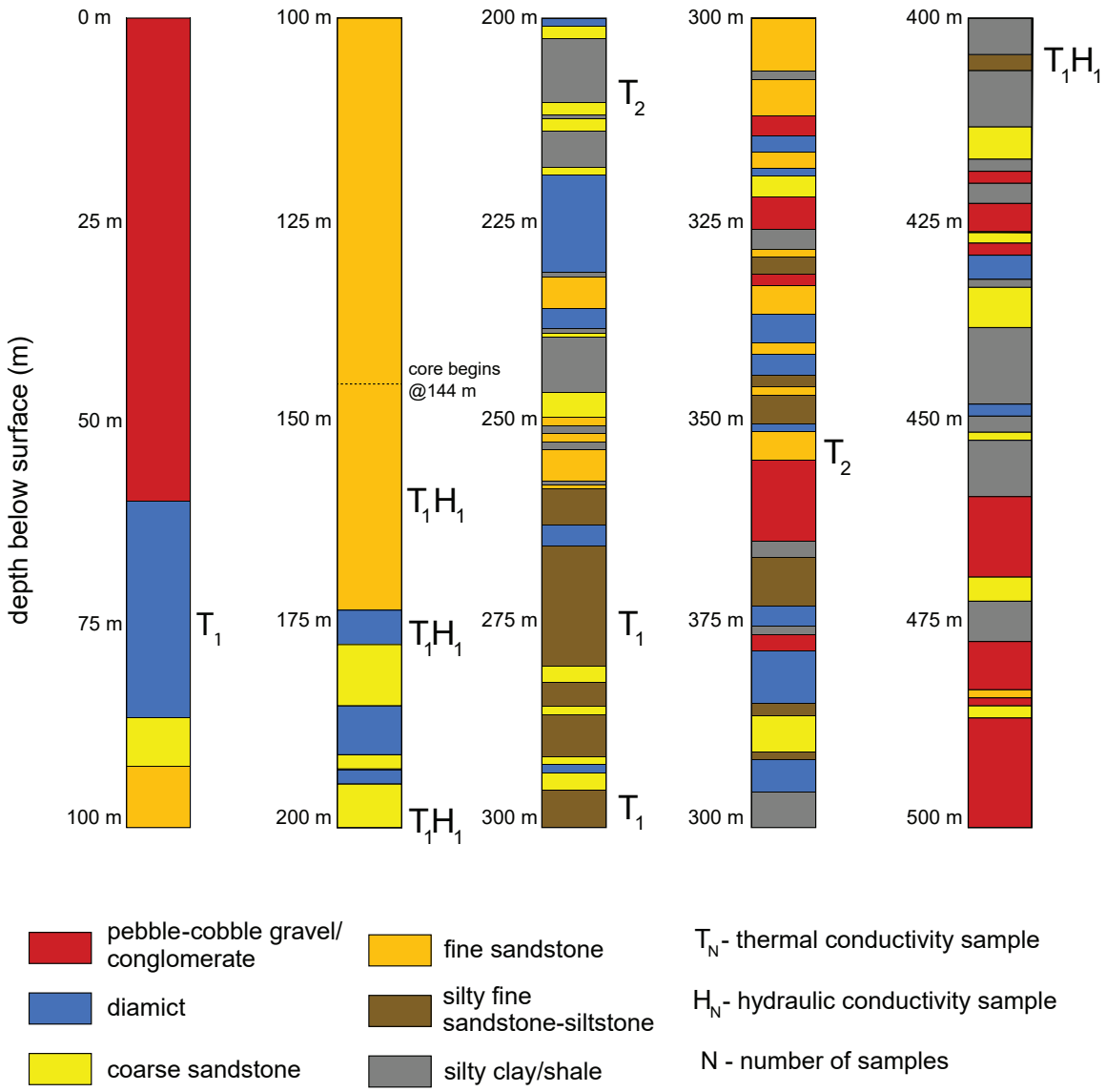

Figure 5. *Lithostratigraphy of the Tintina well (YGS-18-01) including locations of samples for thermal and hydraulic conductivity measurements.*

Figure 6. *Typical condition of core in the Tintina well (YGS-18-01).*

Figure 7. *Outcrop sampling of* ***(a)*** *Upper Triassic Aksala formation (Mandanna member) sandstone near the Takhini drill site and* ***(b)*** *Eocene Flat Creek pluton (granodiorite) west of the Takhini drill site near the end of the Takhini River road.*

Thermal conductivity and diffusivity

Thermal conductivity measures the amount of energy required to transfer a unit of heat through a unit distance of solid material (SI unit $W\,m^{-1}K^{-1}$). This property affects the geothermal gradient when conduction is the dominant heat transfer mechanism. Transient thermal conductivity is measured when the temperature within a material varies over time, whereas steady state thermal conductivity is measured when the temperature within a material is stable. Thermal diffusivity is a property characterizing the thermal inertia of a material at a given temperature (SI unit $m^2\,s^{-1}$), which is essentially quantifying the speed of dispersion of heat within a material from hot to cold. This property affects the geothermal gradient because it characterizes the propagation of thermal disturbances over time such as the effect of past glaciations.

Thermal conductivity measurements on well and outcrop samples were collected using three different instruments. The K2D Pro TR-1 needle probe was used for unconsolidated samples (Fig. 8a). The needle probe is inserted into a sample under ambient conditions, and then is heated at a constant input. Temperature change of the sensor over time, surface area of the needle, and heat input are used to calculate the thermal conductivity of the sample (Decagon Devices, 2012). These parameters are used to calculate transient thermal conductivity for both *in situ* and water saturated conditions according to the ASTM 5334 standard procedure for soil and soft rocks. Only values for saturated conditions are presented in this report as rocks under evaluation are below the groundwater level; however, both *in situ* and saturated measurements are provided in Appendix A3. This instrument has a relative error of 10%. This method was used for five unconsolidated/ brecciated samples from the Tintina well, two from the 'breccia' unit from Takhini well, and three from Quaternary outcrops near the Takhini well.

The Lippmann and Rauen thermal conductivity scanner (TCScan; Fig. 8b) was used for consolidated samples. The scanner measures temperature variations of a sample over time; the sample is heated using a focussed, continuous heat source in combination with infrared temperature sensors (Popov *et al.*, 2020). Thermal conductivity values of studied samples are compared to temperatures obtained in standard samples with known thermal conductivity values. Thermal conductivity values are provided for *in situ* conditions at ambient temperature and have a relative error of ± 5%. The TCScan was used for all consolidated samples from the Tintina and Takhini wells, and Takhini outcrop samples (number of samples = 6, 41 and 39, respectively).

Measurements of steady-state (*i.e.*, set temperature) thermal conductivity were conducted on a small subset of consolidated samples using the FOX50 guarded heat flow meter (Fig. 8c). Based on Fourier's Law, the FOX50 measures heat flux, sample thickness, and temperature differences across the sample to determine thermal conductivity at set temperatures ranging from -10 to 190°C for *in situ* and water saturated conditions (Lasercomp-TA Instruments, 2020). For this study, measurements were only made for *in situ* conditions as sample porosity was low, and thermal conductivity was evaluated at temperatures between 20 and 160°C. Conductive thermal pads were placed on each side of the sample to guarantee thermal contact between the plates and the sample. FOX50 measurements have a relative error of ± 10% with thermal pads. This instrument was used for one or two representative consolidated samples for each geological unit in the vicinity of the Takhini well (n = 15) and one from a felsic plutonic rock in the well at a depth of 370.3–370.5 m, to determine exponential expressions relating thermal conductivity and temperature.

Thermal diffusivity was measured on consolidated well (Tintina = 6; Takhini = 41) and outcrop (Takhini region = 39) samples using the TCScan. An additional infrared temperature sensor, located 7 mm from the heated scan line, allows for the measurement of heat dispersion through the sample at the same time as

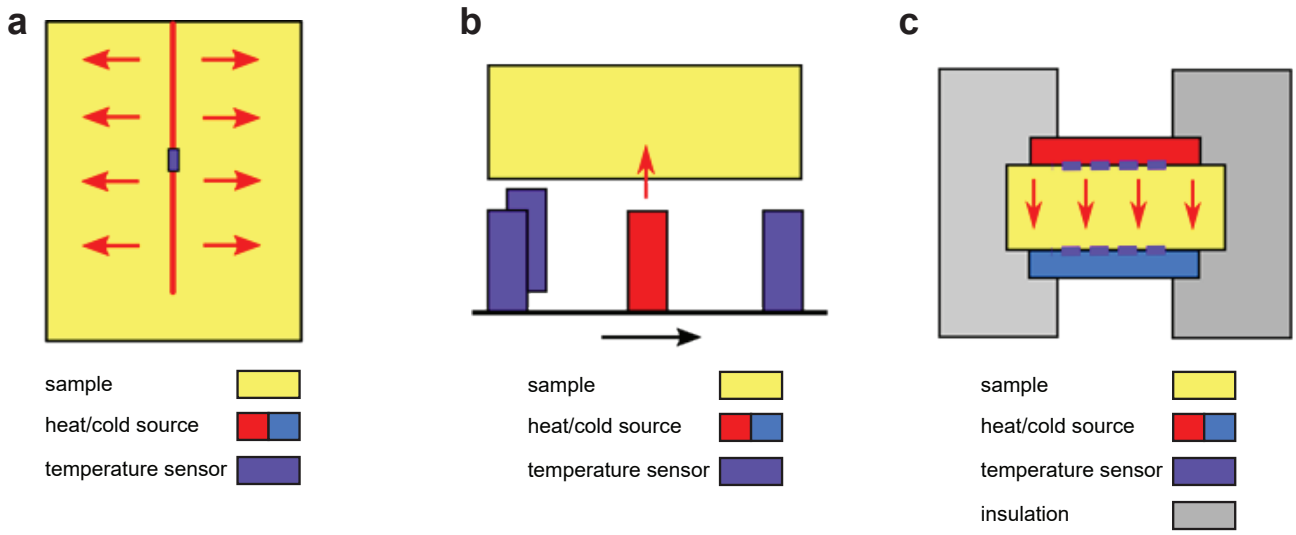

Figure 8. *Schematic diagrams of instruments used to measure thermal conductivity. Heat propogration is shown by the red arrows.* ***(a)*** *the K2D Pro TR-1 needle probe for unconsolidated rocks (Decagon Devices Inc., 2012),* ***(b)*** *the Lippmann and Rauen TCScan for consolidated samples (Popov et al., 2020) and* ***(c)*** *the FOX50 heat flow meter for consolidated samples (Lasercomp-TA instruments, 2020).*

it records temperature for thermal conductivity. The sensors, 7 mm apart, measure temperature of the sample at given points both on and off the heated scanline to determine of heat dispersion (thermal diffusivity) as proposed by the equation of Popov *et al.* (2020). Thermal conductivity and diffusivity values in this study are reported as a range of ± 2 standard deviations (σ) within a ~95% level of confidence around the lithological unit averages, and units with a single sample have an error of ± 10% (Appendix A4). All raw thermal conductivity and diffusivity data are tabulated in Appendices A1 to A3.

Relationship between thermal conductivity and temperature

Thermal conductivity of rocks varies with depth due to temperature changes and lithospheric pressure (Sass *et al.,* 1992; Vosteen and Schellschmidt, 2003; Langevin *et al*., 2019). The relationships between thermal conductivity and temperature for geological units were determined for outcrop samples in the Takhini area.

The relationship between thermal conductivity and temperature is expressed as an exponential equation:

$$\lambda(T) = \lambda_0 \, e^{aT} \qquad (1)$$

where $\lambda(T)$ is the thermal conductivity at temperature T ($W\,m^{-1}\,K^{-1}$), λ_0 is the thermal conductivity at 0°C ($W\,m^{-1}\,K^{-1}$), a is the decay rate of thermal conductivity ($°C^{-1}$) and T is the temperature (°C). Relationships were compared to well-known empirical equations from Vosteen and Schellschmidt (2003) describing the decay rate for igneous, metamorphic and sedimentary rocks (Fig. 9). Equations of Vosteen and Schellschmidt (2003) are $\lambda(T) = 2.3e^{0,0009T}$ where a ranges from -0.0040 to 0.0024 for igneous rocks; $\lambda(T) = 2.6e^{0,0010T}$ where a ranges from -0.0060 to 0.0031 for metamorphic rocks; and $\lambda(T) = 2.9e^{0,0020T}$ where a ranges from -0.0050 to 0.0012 for sedimentary rocks.

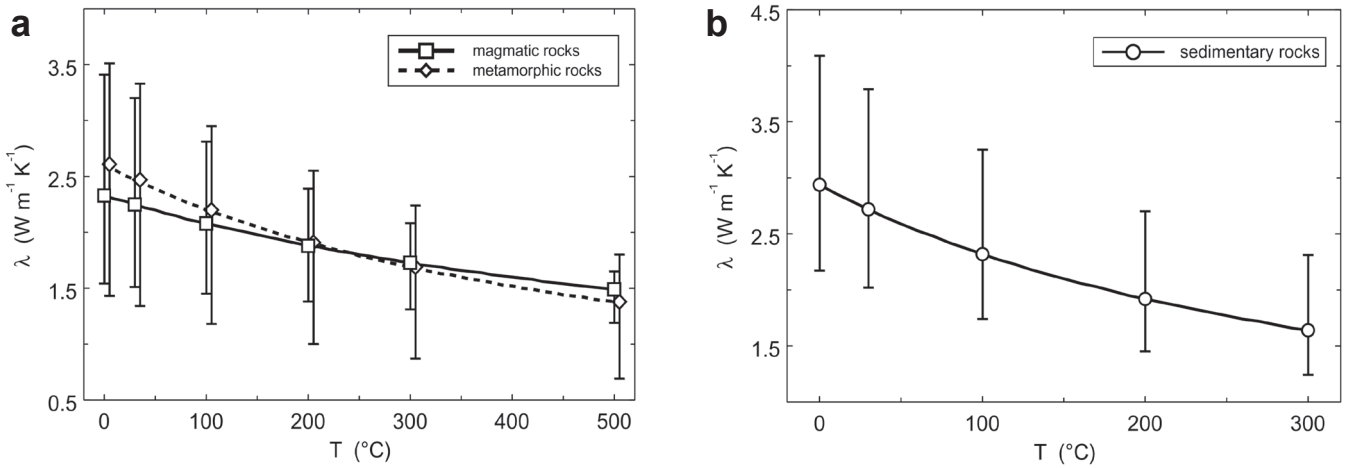

Figure 9. *Relationships between thermal conductivity and temperature from Vosteen and Schellschmidt (2003):* ***(a)*** *igneous and metamorphic rocks and* ***(b)*** *sedimentary rocks.*

Radiogenic heat production

Radiogenic heat production is a parameter characterizing the internal energy produced by radioactive decay in a cubic meter of material (SI unit W m^{-3}). Thirty-three samples from the Takhini well and outcrops were sent to ALS labs in Vancouver for whole rock geochemical analysis to determine concentrations of U, Th, and K, the primary radioactive elements present in rocks. Additionally, geochemical data from four Povoas formation basalt samples from Bordet *et al.* (2019) were added to the data set. Concentrations were converted to radiogenic heat production *A* (μW m^{-3}) using the Rybach (1981) method:

$$A = 10^{-5} \cdot \rho \cdot (9.52[U] + 2.56[Th] + 3.48[K]) \quad (2)$$

where ρ is the rock density (kg m^{-3}), [U] is the uranium concentration (ppm), [Th] is the thorium concentration (ppm), and [K] is the potassium concentration (%).

Values are reported as ranges of ± 2 standard deviations (σ) within a ~95% level of confidence around the lithological unit averages (μ). Radiogenic heat production values in this study are reported as a range of ± 2 standard deviations (σ) within a ~95% level of confidence around the lithological unit averages, and units with a single sample have an error of ± 10% (Appendix B3). All raw geochemistry data are provided in Appendix B1, and individual sample heat production values are provided in Appendix B2.

Hydraulic conductivity

Hydraulic conductivity is the ability of a material to transmit fluid through pore spaces or fractures under a hydraulic gradient, expressed as a distance over a given period of time (SI units m s^{-1}). For this study, three different methods to evaluate hydraulic conductivity were used, depending upon the sample's state of consolidation and fracture.

Consolidated rocks

Air permeability of consolidated core plugs was evaluated using a transient gas permeameter (Core Lab Instruments, 2016; measured in milliDarcies or mD). This instrument forces compressed air through a 4 cm diameter by 8 cm long core, and measures the pressure decay as the air infiltrates the rock (Fig. 10). Recorded pressures are then plotted as a function of time to calculate air permeability. Permeability values were converted to hydraulic conductivity using a factor of 1 mD = 9.6 × 10^{-9} m s^{-1} (Duggal and Soni, 1996), assuming water density and viscosity at ambient temperature. The transient gas permeameter was used to analyze 21 cores from the Takhini well and 16 samples from outcrops near Takhini Hot Springs. From two to four runs were made on each sample and the average hydraulic conductivity of the runs assigned to each sample, except in instances where there was a misrun due to gas leakage. The instrument has a permeability measurement range of 0.01 to 5000 mD (9.6 × 10^{-11} to 4.8 × 10^{-5} m s^{-1}) under ideal operating conditions.

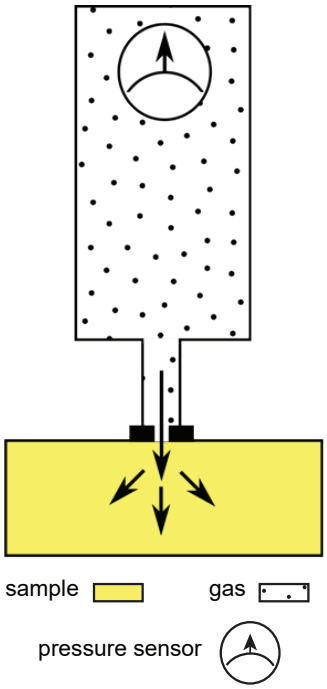

Figure 10. *Schematic of the transient gas permeameter which is used to measure and record pressure decay as the air infiltrates consolidated rocks to calculate air permeability.*

However, measurements in the range of 1 to 2 mD (9.6×10^{-9} to 1.9×10^{-8} m s^{-1}) were assigned a value <1 mD (< 9.6×10^{-9} m s^{-1}) due to difficulties in keeping rock surfaces pressurized. The hydraulic conductivity evaluated for plugs analyzed by the gas permeameter are related to primary porosity, or porosity that existed when the rock was originally formed.

Hydraulic conductivity of unconsolidated/ brecciated rocks

Hydraulic conductivity was evaluated on two unconsolidated rock samples from a major breccia/ fault zone in the Takhini well at a depth of 345 to 346 m. Four samples from the Tintina well were also evaluated for hydraulic conductivity, at depths of 161.0, 174.3, 199.3, and 405.8 m.

The hydraulic conductivity K (m s^{-1}) for an unconsolidated and/or strongly brecciated sample was calculated based on the empirical equation of Beyer (1966) using the grain size distribution of the rock (Alvarado Blohm *et al.*, 2016):

$$K = \frac{g}{v} \cdot 6 \times 10^{-4} \cdot \left(\log\left[\frac{500}{d_{60}/d_{10}}\right]\right) \cdot d_{10}^{2} \quad (3)$$

where g is the gravitational acceleration (m s^{-2}); v is the kinematic viscosity of water (10^{-6} m^2 s^{-1}); and d_{10} and d_{60} are the diameters (m) of the 10% and 60% passing particle size. The method assumes that the hydraulic conductivity of unconsolidated rocks is related to grain size distribution affecting pore connections, where smaller grains can fill voids between larger grains. The hydraulic conductivity values reported from this method represent bulk values.

Fractured rocks

Depending on the degree of deformation and inherent mechanical properties, rocks can be highly fractured at depth, providing preferential paths for groundwater flow. Fracture aperture and spacing can be used to calculate hydraulic conductivity K (m s^{-1}) using the Cubic law, which is associated with secondary porosity (Witherspoon *et al.*, 1979):

$$K = \frac{\rho \cdot g \cdot (b)^3 \cdot N}{12 \cdot \mu} \quad (4)$$

where ρ is the density of the rock matrix (kg m^{-3}); g is the gravitational acceleration (m s^{-2}); b is the width of the fracture (m); N is the total number of fractures per metre (m^{-1}); and μ is the dynamic viscosity of water (10^{-3} kg s^{-1} m^{-1}).

This method requires a manual count of natural fractures per unit distance (N) on cores and an estimation of fracture aperture (b; Fig. 11). Care must be taken not to count fractures that have occurred during or post drilling. Each open fracture having mineralization observed in the Takhini core (*e.g.*, calcite, pyrite or chlorite precipitate) was assumed to be natural (Fig. 12). Fracture aperture was not measured in core, as the measurements would not reflect *in situ* conditions. Instead, aperture was assigned a constant value for the entire well bore and the calculations were made for three aperture types: superfine, fine, or moderate-large. Superfine assigned apertures range from 0.2 to 4 µm; fine assigned apertures from 4 to 100 µm; and moderate to large are assigned a range of 100 to 3000 µm, based

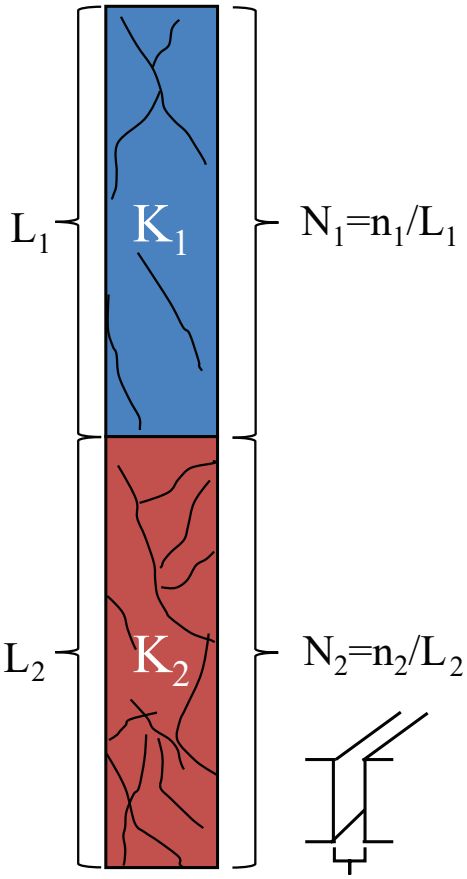

Figure 11. *Measured parameters for calculating hydraulic conductivity on fractured rocks using the Cubic law where 'n' is the number of fractures, 'L' is length of the geological unit (m), 'N' is the number of fractures per unit metre (m^{-1}), and 'b' is the fracture width (m).*

on studies by Witherspoon *et al*. (1979). Hydraulic conductivity values ($m\ s^{-1}$) therefore are reported as ranges for each aperture type, with the number of fractures per unit distance (*N*), the only variable in the equation (Fig. 11). Further, this method assumes that fractures are interconnected and groundwater is flowing in every fracture observed. This method of determining hydraulic conductivity was evaluated for the entire Takhini well core (55–500 m depth).

Takhini geological cross sections

Two geological cross sections were drawn through the Takhini well bore to help understand groundwater flow and heat transfer in the Takhini area. Cross sections were made using data from existing geological maps (Yukon Geological Survey, 2018a,b), and core from the Takhini well and selected outcrop samples. The cross section extents were determined by the position of strategic water bodies such as the Takhini River, Takhini Hot Springs, Lake Laberge and Kusawa Lake as they represent flow boundaries (Fig. 13). Thermo-hydraulic properties measured from samples in the well and from outcrops were used to define potential regional ranges of values. All data were interpreted to define a hydrothermal conceptual model of the region.

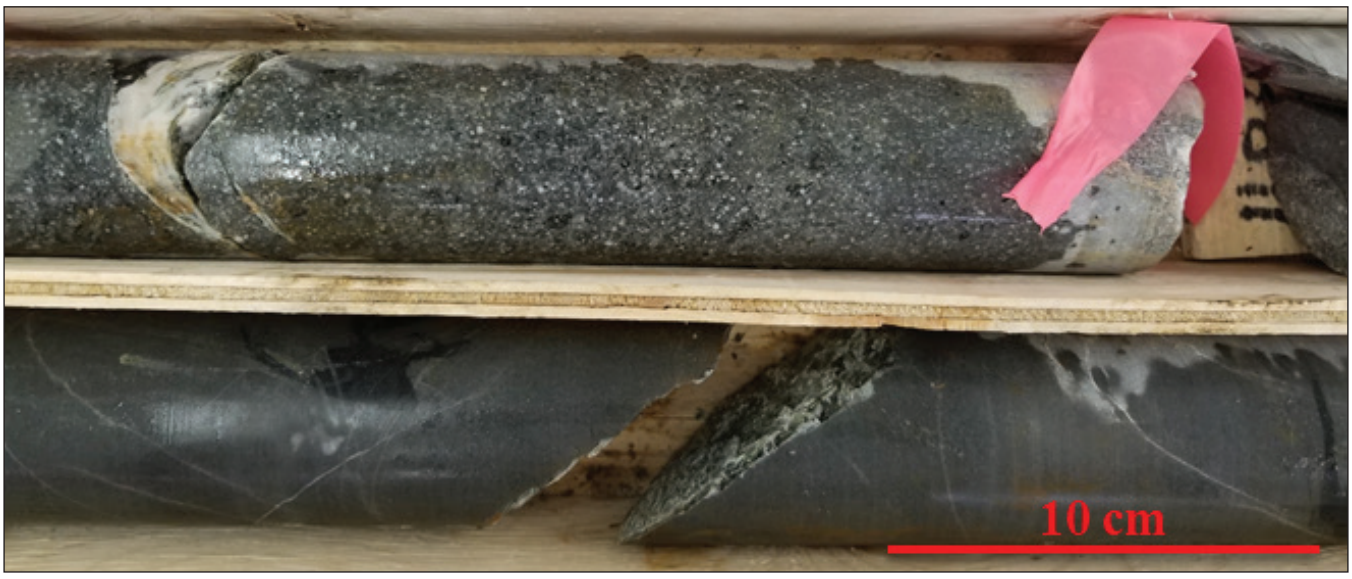

Figure 12. *Volcaniclastic coarse sandstone in the Takhini well (YGS-17-01; 487m) crosscut by a calcite vein (upper core) and shale crosscut by an open fracture lined with calcite and chlorite precipitates (lower core; 489 m).*

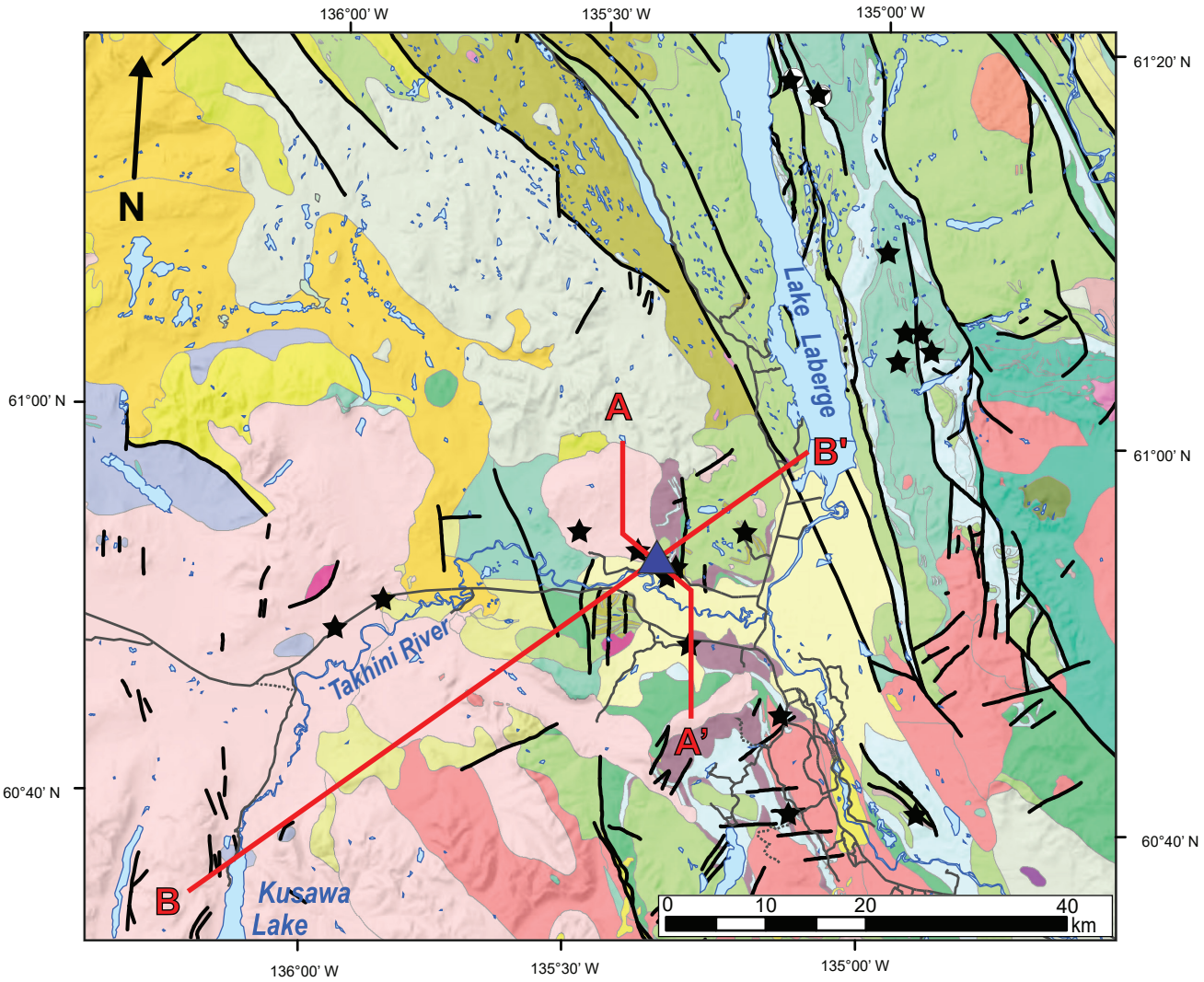

LEGEND

- roads
- well location
- sampled outcrop
- cross section
- waterbody
- fault

Layered rocks

Cenozoic
- Quaternary
- volcanics

Mesozoic

Upper Cretaceous
- Carmacks Gp volcanics

Upper Jurassic – Lower Cretaceous
- Tantalus Fm

Jurassic
- Richthofen fm
- Nordenskiold fm

Triassic
- Mandanna mbr
- Hancock mbr
- Casca mbr
- Povoas fm

Paleozoic

Pennsylvanian and older
- Takhini assemblage

Upper Devonian and older
- Snowcap assemblage

Plutonic rocks
- Paleocene–Eocene
- Late Cretaceous
- Early Cretaceous
- Middle Jurassic
- Early Jurassic
- Triassic

Figure 13. *Geological map in the vicinity of the Takhini well (YGS-17-01), and location of cross sections shown in Figure 19. Geology from Yukon Geological Survey (2018a).*

Results

Takhini area

Thermal properties in YGS-17-01 (well samples)

Average and ranges of thermal conductivity, radiogenic heat production, and thermal diffusivity for the Takhini well are shown in Table 1. Complete raw and average/range data sets of the thermal conductivity/diffusivity and radiogenic heat production are in Appendices A and B, respectively.

Average thermal conductivity values (± 2σ or 10%) per lithological unit in the well range from 0.59 to 4.19 W m^{-1} K^{-1}; the highest average value is in the deformed sandstone and shale unit (3.81 W m^{-1} K^{-1}), and the lowest average value is in the fault/breccia unit (0.97 W m^{-1} K^{-1}). Generally, average values are similar in the well and range between 3.0 and 4.0 W m^{-1} K^{-1}, except for the mafic dike and the fault/breccia units, which have values ≤2.4 W m^{-1} K^{-1}. Note that there are no data for the 'pebbly volcaniclastic sandstone and tuff' and 'volcaniclastic sandstone and mafic tuff' units, as the rock properties were deemed similar to the 'volcaniclastic sandstone, minor interbedded siltstone and shale' and 'pebbly volcaniclastic sandstone' units of which 14 and 3 samples were taken, respectively.

Average radiogenic heat production values (± 2σ or 10%) per lithological unit in the well range from 0.39 to 3.60 µW m^{-3}; the highest average value is in the 'felsic dike' unit (2.94 µW m^{-3}), and the lowest average value is in the 'mafic dike' unit (0.63 µW m^{-3}). Generally, average values are <1 µW m^{-3}, except for the felsic dike unit. Note that there are no data for the 'deformed sandstone and shale', 'interbedded shale and sandstone' and breccia units, as these units occur in insignificant proportions in the well.

Average thermal diffusivity values (± 2σ or 10%) per lithological unit in the well range from 0.96 to 2.98 mm^2 s^{-1}; the highest average value is in the interbedded shale and sandstone unit (2.07 mm^2 s^{-1}), and the lowest average value is in the mafic dike unit (1.08 mm^2 s^{-1}). Generally, average values are between 1 and 2 mm^2 s^{-1}. Note that there are no data for the 'pebbly volcaniclastic sandstone and tuff' and 'volcaniclastic sandstone and mafic tuff' units, as the rock properties were deemed similar to the 'volcaniclastic sandstone, minor interbedded siltstone and shale' unit and the 'pebbly volcaniclastic sandstone' of which 14 and 3 samples were taken, respectively. The breccia unit was not analyzed as the rock was incompetent and could not be used on the TCScan.

Thermal properties in outcrop samples

Average and range for thermal conductivity, radiogenic heat production, and thermal diffusivity for outcrops in the Takhini area are shown in Table 2. Complete data sets of the thermal conductivity/diffusivity and radiogenic heat production are in Appendices A and B, respectively.

Average thermal conductivity values (± 2σ or 10%) per lithological unit for outcrop samples range from 0.73 to 4.14 W m^{-1} K^{-1}; the highest average value is in the Hancock unit (3.18 W m^{-1} K^{-1}), and the lowest average value is in the Quaternary silt unit (1.07 W m^{-1} K^{-1}). Average values of pre-Quaternary rocks range between 2.0 and 3.5 W m^{-1} K^{-1}.

Radiogenic heat production values (± 2σ or 10%) per lithological unit for Takhini outcrop samples ranges from 0.00 to 3.46 µW m^{-3}, the highest average value is in the Flat creek pluton (3.00 µW m^{-3}), and the lowest average value is in the Takhini assemblage (0.11 µW m^{-3}). All average values are <1 µW m^{-3}, except for igneous rocks of the Ruby Range suite (Annie Ned batholith and Flat Creek pluton).

Thermal diffusivity values (± 2σ or 10%) per lithological unit for Takhini outcrop samples ranges from 0.50 to 2.62 mm^2 s^{-1}; the highest average value is in the limestone of the Hancock member (1.56 mm^2 s^{-1}), and the lowest average value is in the Takhini assemblage metasediments (0.89 mm^2 s^{-1}). Generally, average values range between 1.0 and 1.6 mm^2 s^{-1}.

Table 1. *Thermal properties of the Takhini well (YGS-17-01).*

lithology description	lithology graphic	Thermal conductivity				Radiogenic heat production				Thermal diffusivity			
		number of samples	average ($Wm^{-1}K^{-1}$)	standard deviation (σ)	low; high (± 2σ or 10%; $Wm^{-1}K^{-1}$)	number of samples	average ($\mu W\ m^{-3}$)	standard deviation (σ)	low; high (± 2σ or 10%; μWm^{-3})	number of samples	average ($mm^2\ s^{-1}$)	standard deviation (σ)	low; high (± 2σ or 10%; $mm^2\ s^{-1}$)
deformed sandstone and shale		1	3.28	-	2.95; 3.61	0	-	-	-	1	1.50	-	1.35; 1.65
carbonate altered sandstone to pebbly sandstone		3	3.47	0.21	3.05; 3.89	2	1.00	0.04	0.92; 1.08	3	1.54	0.14	1.26; 1.82
felsic dike		5	3.38	0.1	3.18; 3.58	4	2.94	0.33	2.28; 3.60	5	2.00	0.49	1.02; 2.98
interbedded shale and sandstone		1	3.81	-	3.43; 4.19	0	-	-	-	1	2.07	-	1.86; 2.28
shale and fine sandstone		7	3.16	0.42	2.32; 4.00	3	1.30	0.31	0.68; 1.92	7	1.38	0.13	1.12; 1.64
pebbly volcaniclastic sandstone		3	3.16	0.07	3.02; 3.30	3	0.88	0.06	0.76; 1.00	3	1.49	0.21	1.07; 1.91
intermediate dike		2	3.06	0.01	3.04; 3.08	1	1.04	-	0.94; 1.14	2	1.29	0.02	1.25; 1.33
volcaniclastic sandstone, minor interbedded siltstone and shale		14	2.94	0.15	2.64; 3.24	5	1.00	0.24	0.52; 1.48	14	1.35	0.12	1.11; 1.59
mafic dike		5	2.39	0.12	2.15; 2.63	3	0.63	0.12	0.39; 0.87	5	1.08	0.06	0.96; 1.20
fault/breccia		2	0.98	0.19	0.63; 1.33	0	-	-	-	2	-	-	-
pebbly volcaniclastic sandstone and tuff		0	-	-	-	1	0.73		0.66; 0.80	0	-	-	-
volcaniclastic sandstone and mafic tuff		0	-	-	-	2	0.91	0.17	0.57; 1.25	0	-	-	-

Table 2. *Thermal properties of outcrop samples in the Takhini area.*

Stratigraphy			Thermal conductivity				Radiogenic heat production				Thermal diffusivity			
group	formation	member	number of samples	average ($W\ m^{-1}\ K^{-1}$)	standard deviation (σ)	low; high (± 2σ or 10%; $Wm^{-1}K^{-1}$)	number of samples	average ($\mu W\ m^{-3}$)	standard deviation (σ)	low; high (± 2σ or 10%; $\mu W\ m^{-3}$)	number of samples	average ($mm^2\ s^{-1}$)	standard deviation (σ)	low; high (± 2σ or 10%; $mm^2\ s^{-1}$)
Quaternary			2	1.07	0.17	0.73; 1.41	0	-	-	-	0	-	-	-
Ruby Range	Flat Creek pluton		3	2.53	0.62	1.29; 3.77	4	3.00	0.23	2.54; 3.46	3	1.24	0.20	0.84; 1.64
Ruby Range	Annie Ned Batholith		2	2.39	0.23	1.93; 2.85	1	1.66	-	1.49; 1.83	2	1.16	0.17	0.82; 1.50
Laberge	Nordenskiöld		2	2.80	0.41	1.98; 3.62	0	-	-	0.46; 1.26	2	1.27	0.13	1.01; 1.53
Laberge	Richthofen		4	2.70	0.05	2.60; 2.80	0	-	-	0.66; 1.66	4	1.21	0.06	1.09; 1.33
Lewes River	Aksala	Hancock	7	3.18	0.48	2.22; 4.14	1	0.22	-	0.20; 0.24	7	1.56	0.53	0.50; 2.62
Lewes River	Aksala	Mandanna	6	2.55	0.17	2.21; 2.89	1	0.59	-	0.53; 0.65	6	1.15	0.06	1.03; 1.27
Lewes River	Aksala	Casca	5	2.53	0.30	1.93; 3.13	1	0.72	-	0.65; 0.79	5	1.09	0.11	0.87; 1.31
Lewes River	Povoas		6	2.49	0.35	1.79; 3.19	3	0.10	-	0.00; 0.34	6	1.08	0.16	0.76; 1.40
Takhini assemblage			5	2.07	0.09	1.89; 2.25	1	0.11	-	0.10; 0.12	5	0.89	0.10	0.69; 1.09

Hydraulic conductivity

Average hydraulic conductivity values for consolidated rock samples in the Takhini well and from nearby outcrops are shown in Tables 3a and 3b, respectively, with a full data set and calculations provided in Appendix C1. Gas permeameter measurements indicate a hydraulic conductivity $<9.6 \times 10^{-9}$ m s^{-1} for all but eight samples (four well and four outcrop samples). The maximum average hydraulic conductivity occurs in a mafic dike sample at a depth of ~424.6 m in the Takhini well, with a value of 1.6×10^{-7} m s^{-1}, which is an order of magnitude or more than all other samples (the rest are $\leq 9.3 \times 10^{-8}$ m s^{-1}).

Hydraulic conductivity values for two brecciated rock samples at the 345–346 m depth in the well were evaluated at 8.3×10^{-4} and 2.9×10^{-4} m s^{-1} (Table 4; Fig. 14), averaging 5.6×10^{-4} m s^{-1}. Fracture spacing ranges from 2 to 52 fractures per metre along the well, typical values are <10 (Fig. 4); values of fracture-related hydraulic conductivity are shown in Figure 15. Overall, hydraulic conductivity values are on the order of 10^{-14} m s^{-1}, 10^{-10} m s^{-1}, and 10^{-6} and 10^{-1} m s^{-1} for superfine, fine and moderate to large apertures, respectively.

Table 3. *Hydraulic conductivity of consolidated rock samples in* ***(a)*** *the Takhini well (YGS-17-01) and* ***(b)*** *outcrop samples in the Takhini region.*

a

well lithological unit	sample lithology	well depth from (m)	well depth to (m)	hydraulic conductivity (m s^{-1})
	volcaniclastic sandstone	302.83	303.07	<9.6x10^{-9}
	volcaniclastic sandstone	325.16	325.34	<9.6x10^{-9}
	fine sandstone with shale	363.17	363.32	<9.6x10^{-9}
	mafic intrusive	378.89	379.09	2.8x10^{-8}
	fine sandstone with minor shale	401.86	402.08	<9.6x10^{-9}
	mafic intrusive	423.03	423.18	<9.6x10^{-9}
	mafic intrusive	424.58	424.76	1.6x10^{-7}
	fine sandstone minor shale	439.86	440.00	7.1x10^{-8}
	fine sandstone minor shale	455.00	455.25	<9.6x10^{-9}
	fine sandstone minor shale	459.43	459.27	<9.6x10^{-9}
	fine sandstone minor shale	461.44	461.59	2.1x10^{-8}
	volcaniclastic sandstone	462.85	463.00	<9.6x10^{-9}
	volcaniclastic sandstone	467.00	467.15	<9.6x10^{-9}
	intermediate intrusive	470.39	470.59	<9.6x10^{-9}
	intermediate intrusive	475.00	475.28	<9.6x10^{-9}
	fine sandstone with shale	480.38	480.52	<9.6x10^{-9}
	fine sandstone with shale	485.95	486.10	<9.6x10^{-9}
	volcaniclastic sandstone	493.10	493.25	<9.6x10^{-9}
	volcaniclastic sandstone	496.40	496.50	<9.6x10^{-9}
	fine sandstone with minor shale	497.00	497.15	<9.6x10^{-9}
	volcaniclastic sandstone	497.84	498.00	<9.6x10^{-9}

b

sample number	latitude	longitude	lithology	formation	hydraulic conductivity (m s^{-1})
19-TF-01-2	60.89	-135.38	Volcaniclastic sandstone	Nordenskiöld	<9.6x10^{-9}
19-TF-02-1	60.89	-135.41	Granite	Flat creek pluton	<9.6x10^{-9}
19-TF-04-1	60.89	-135.37	Sandstone	Aksala (Mandanna mbr)	9.3x10^{-8}
19-TF-04-2	60.89	-135.37	Siltstone	Aksala (Mandanna mbr)	<9.6x10^{-9}
19-TF-06-1	60.92	-135.22	Sandstone	Richthofen	<9.6x10^{-9}
19-TF-06-3	60.92	-135.22	Sandstone	Richthofen	<9.6x10^{-9}
19-TF-07-1	60.91	-135.52	Leucogranite	Flat creek pluton	9.3x10^{-8}
19-TF-08-1	60.88	-135.35	Fine sandstone	Aksala (Casca mbr)	<9.6x10^{-9}
19-TF-08-2	60.88	-135.35	Fine sandstone	Aksala (Casca mbr)	<9.6x10^{-9}
19-TF-09-1	60.81	-135.97	Granodiorite	Annie Ned batholith	<9.6x10^{-9}
19-TF-10-3	60.84	-135.87	Green schist	Takhini Assemblage	<9.6x10^{-9}
19-TF-11-1	60.82	-135.31	Sandstone	Aksala (Mandanna mbr)	<9.6x10^{-9}
19-TF-GM-1	60.67	-134.90	Limestone	Aksala (Hancock mbr)	<9.6x10^{-9}
15-EB-466-1	61.08	-134.89	Volcanoclastic sandstone	Aksala (Hancock mbr)	7.9x10^{-8}
15-EB-503-1	61.07	-134.95	Pyroclastic basalt	Povoas	<9.6x10^{-9}
17-EB-214-1	61.37	-135.22	Pyroclastic basalt	Povoas	5.1x10^{-8}

Table 4. *Hydraulic conductivity of the breccia unit in the Takhini well (YGS-17-01) and from selected samples in the Tintina well (YGS-18-01) using the size distribution of the rock (Alvarado Blohm et al., 2016). The d_{10} and d_{60} values indicate the grain size, which corresponds to 10% or 60% of the sample weight that is smaller than the indicated grain size.*

well name	sample depth from (m)	sample depth to (m)	lithology	d_{10} (m)	d_{60} (m)	hydraulic conductivity (m s^{-1})
YGS-17-01	345.32	345.52	breccia	0.0002	0.006	2.9×10^{-4}
	346.00	346.20	breccia	0.0003	0.004	8.3×10^{-4}
YGS-18-01	161.00	161.16	fine sand	0.0001	0.0006	1.1×10^{-4}
	174.32	174.54	diamict	0.0007	0.004	5.6×10^{-3}
	199.31	199.56	coarse sand	0.00008	0.00018	8.8×10^{-5}
	405.83	406.15	silty clay	0.00025	0.002	6.6×10^{-4}

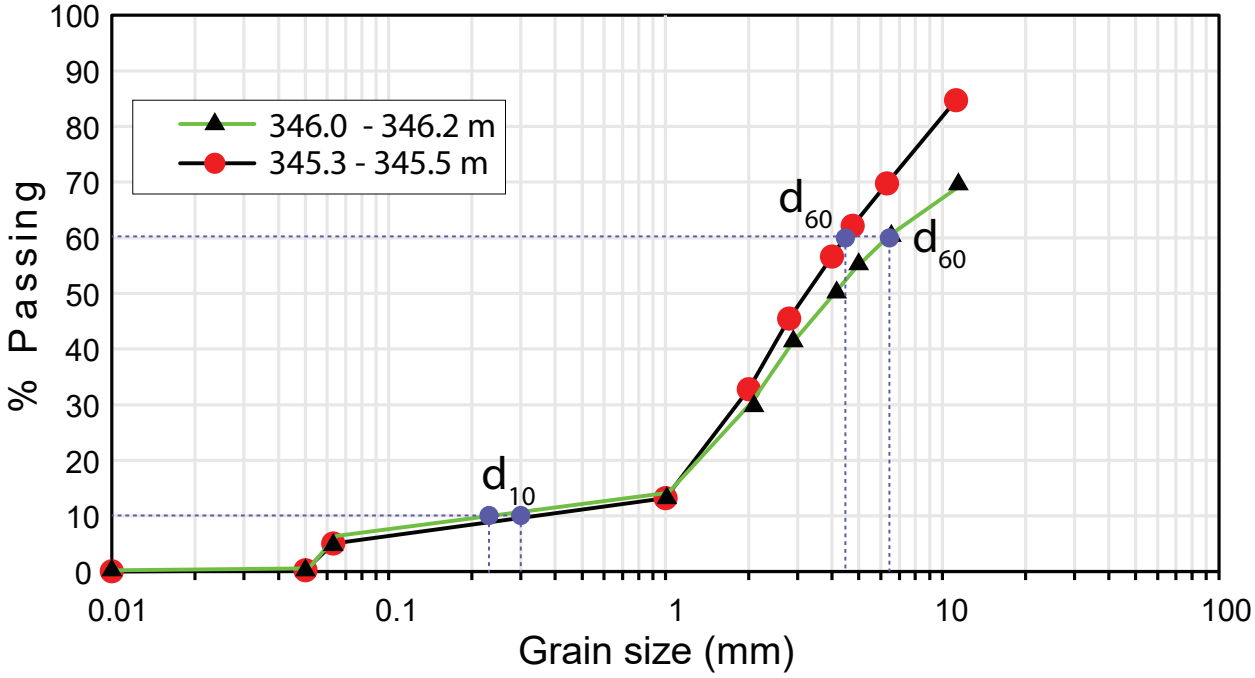

Figure 14. *Grain size distribution of samples from the breccia unit in the Takhini well (YGS-17-01; 346–346.2 m and 345.3–345.5 m). The d_{10} and d_{60} values indicate the grain size, in millimetres, which corresponds to 10% or 60% of the sample weight that is smaller than the indicated grain size. For example, a d_{10} value of 1 mm indicates that 10% of the sample passed through the 1mm sieve size, therefore 10% of the sample < 1mm, and 90% >1 mm.*

The highest value of hydraulic conductivity related to fracture porosity in the Takhini well is found at a depth of 332–341 m in a 'volcaniclastic sandstone with minor interbedded siltstone and shale' unit; 52 fractures per metre were observed (Fig. 4). Hydraulic conductivity for this interval is 3.4×10^{-13} m s^{-1}; 2.7×10^{-9} m s^{-1}; 4.3×10^{-5} and 1.1×10^{0} m s^{-1} for superfine, fine and moderate to large apertures, respectively (Fig. 15). The lowest fracture-related hydraulic conductivity occurs in the lower part of the well at a depth of 465 m in a 'volcaniclastic sandstone with minor interbedded siltstone and shale' unit (Fig. 4), where there are 2.2 fractures per metre. Hydraulic conductivity values calculated for this interval are 1.4×10^{-14} m s^{-1}, 1.2×10^{-10} m s^{-1}, and 1.8×10^{-6} and 4.9×10^{-2} m s^{-1} for superfine, fine, and moderate to large apertures, respectively (Fig. 15).

Relationship between thermal conductivity and temperature of rocks

Relationships between thermal conductivity and temperature on Takhini outcrop samples are shown in Figure 16. The decay rate, or decrease in thermal conductivity with a rise in temperature, *a* ranges from a high of -0.004 for Richthofen formation sedimentary rocks to a low of -0.0008 for Povoas formation volcanic rocks. The decay rate for plutonic rocks ranges from -0.003 to -0.0008; -0.004 to -0.002 for sedimentary rocks; and the decay rate is 0.002 for the metamorphic rocks of the Takhini assemblage. These ranges are comparable to those of Vosteen and Schellschmidt (2003; Fig. 17).

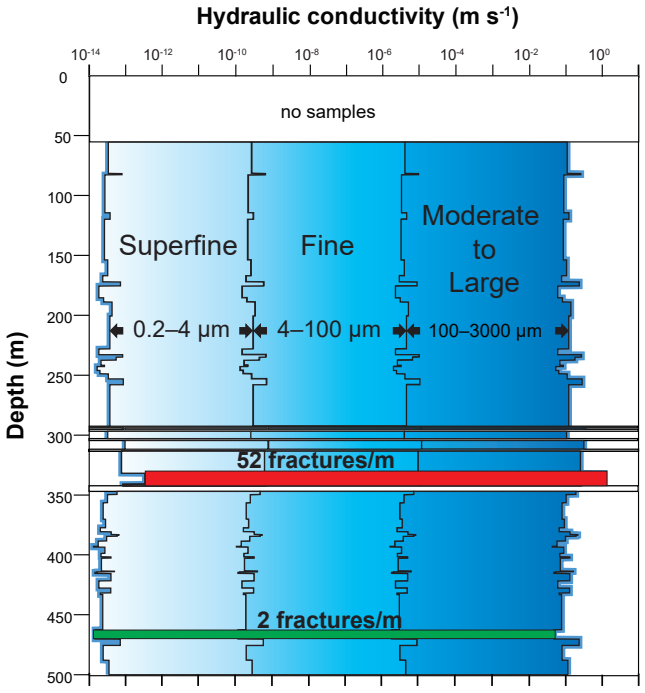

Figure 15. *Hydraulic conductivity of fractured rocks in the Takhini well (YGS-17-01) analyzed for superfine, fine, and moderate-to-large fracture apertures.*

Tintina well (YGS-18-01)

Thermal properties

Thermal conductivity and diffusivity averages and ranges for each geological unit in the Tintina well are presented in Table 5, and complete data sets provided in Appendix A.

Thermal conductivity values in the well (± 2σ or 10%) per lithological unit range from 0.79 to 3.23 W m^{-1} K^{-1}; with both values from the 'coarse sand' unit. The highest average value is in the 'pebble gravel/ conglomerate' unit (2.58 W m^{-1} K^{-1}), and the lowest average value is in the 'fine sand' unit (1.16 W m^{-1} K^{-1}). Thermal diffusivity (± 2σ or 10%) per lithological unit in the well ranges from 0.94 to 1.49 mm^2 s^{-1} from the 'silty clay' and 'coarse sand' units, respectively. The highest average value is in the 'coarse sand' unit (1.35 mm^2 s^{-1}), and the lowest average value is in the 'silty clay' unit (1.04 mm^2 s^{-1}).

Hydraulic conductivity

Grain size distribution for the Tintina well samples are provided in Figure 18, and hydraulic conductivity values are presented in Table 4. A complete set of grain size distribution and hydraulic conductivity calculations can be found in Appendix C2. Poorly consolidated rocks define the Tintina well and hydraulic conductivity values range between 8.8×10^{-5} and 5.6×10^{-3} m s^{-1}. The highest value is in the 'diamict' unit at a depth of 174.54–176.32 m (5.6×10^{-3} m s^{-1}), and the lowest value is in a 'coarse sand' unit at a depth of 199.31–199.56 m (8.8×10^{-5} m s^{-1}).

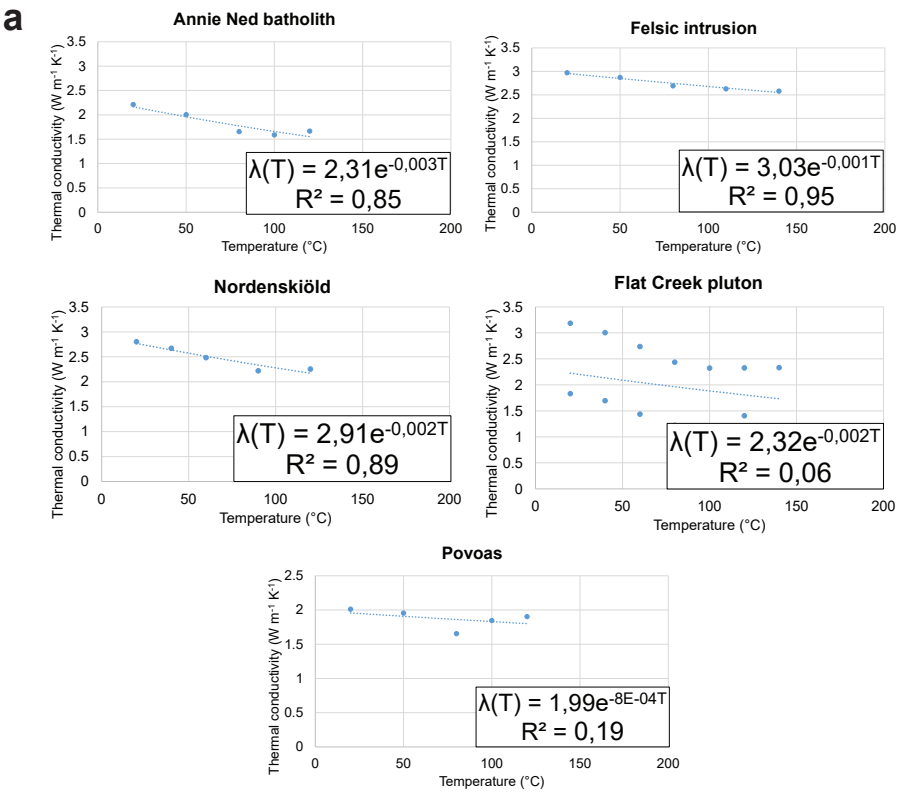

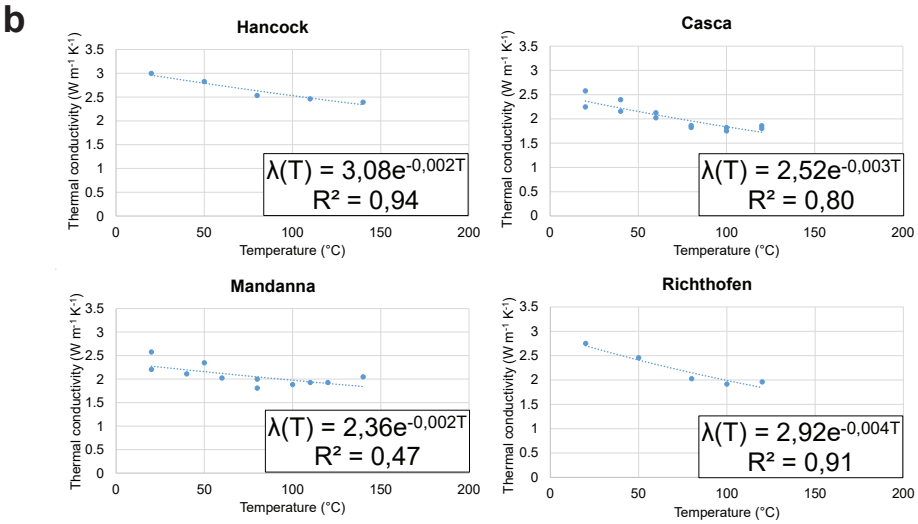

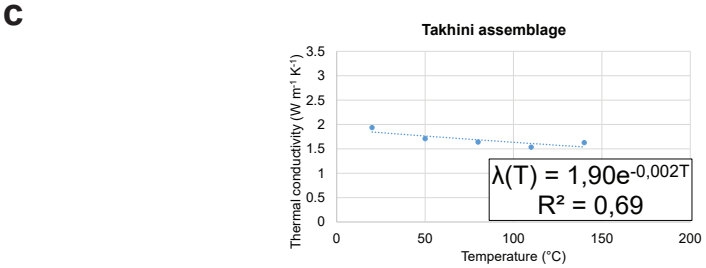

Figure 16. *Relationship between thermal conductivity and temperature for* ***(a)*** *igneous,* ***(b)*** *sedimentary and* ***(c)*** *metamorphic rocks in the Takhini area.*

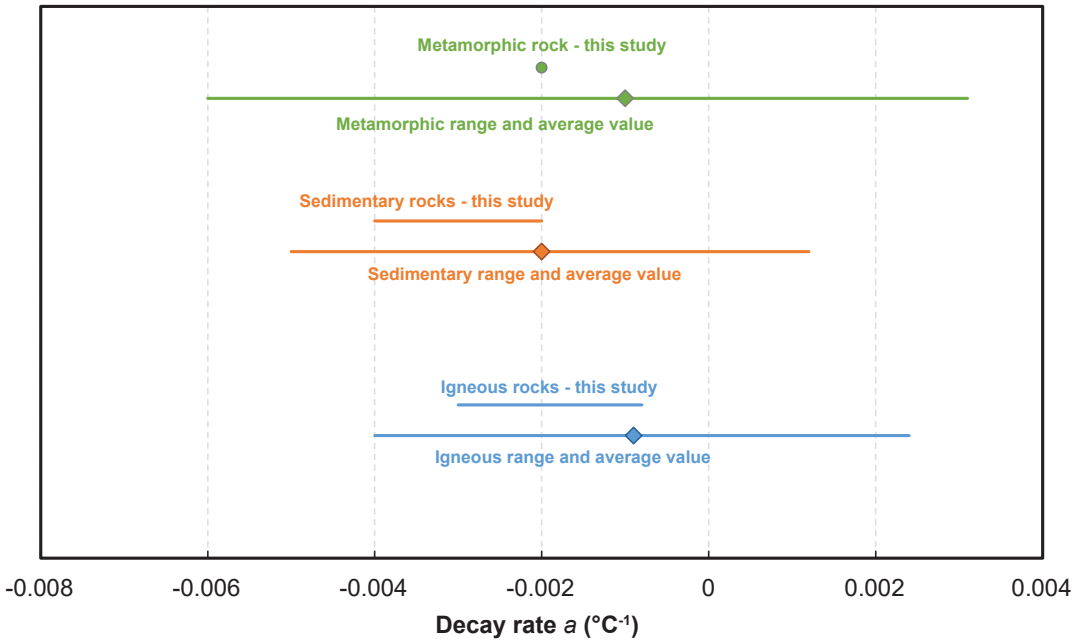

Figure 17. *Comparison between decay rates calculated in this study and those of Vosteen and Schellschmidt (2003) for igneous, sedimentary and metamorphic rocks in the vicinity of the Takhini well.*

Table 5. *Thermal properties of the Tintina well (YGS-18-01).*

lithology description	lithology graphic	Thermal Conductivity				Thermal Diffusivity			
		number of samples	average ($Wm^{-1}K^{-1}$)	standard deviation (σ)	low; high (± 2σ or 10%; $Wm^{-1}K^{-1}$)	number of samples	average ($mm^2 s^{-1}$)	standard deviation (σ)	low; high (± 2σ or 10%; $mm^2 s^{-1}$)
pebble gravel/ conglomerate		2	2.58	0.04	2.50, 2.66	2	1.33	0.04	1.25; 1.41
diamict		2	2.21	0.19	1.83; 2.59	0	-	-	-
coarse sandstone		2	2.01	0.61	0.79; 3.23	1	1.35	-	1.22; 1.49
fine sandstone		1	1.16	-	1.04; 1.28	0	-	-	-
silty fine sandstone - siltstone		2	2.22	0.39	1.44; 3.00	2	1.08	0.04	1.00; 1.16
silty Clay		2	1.85	0.48	0.89; 2.81	1	1.04	-	0.94; 1.14

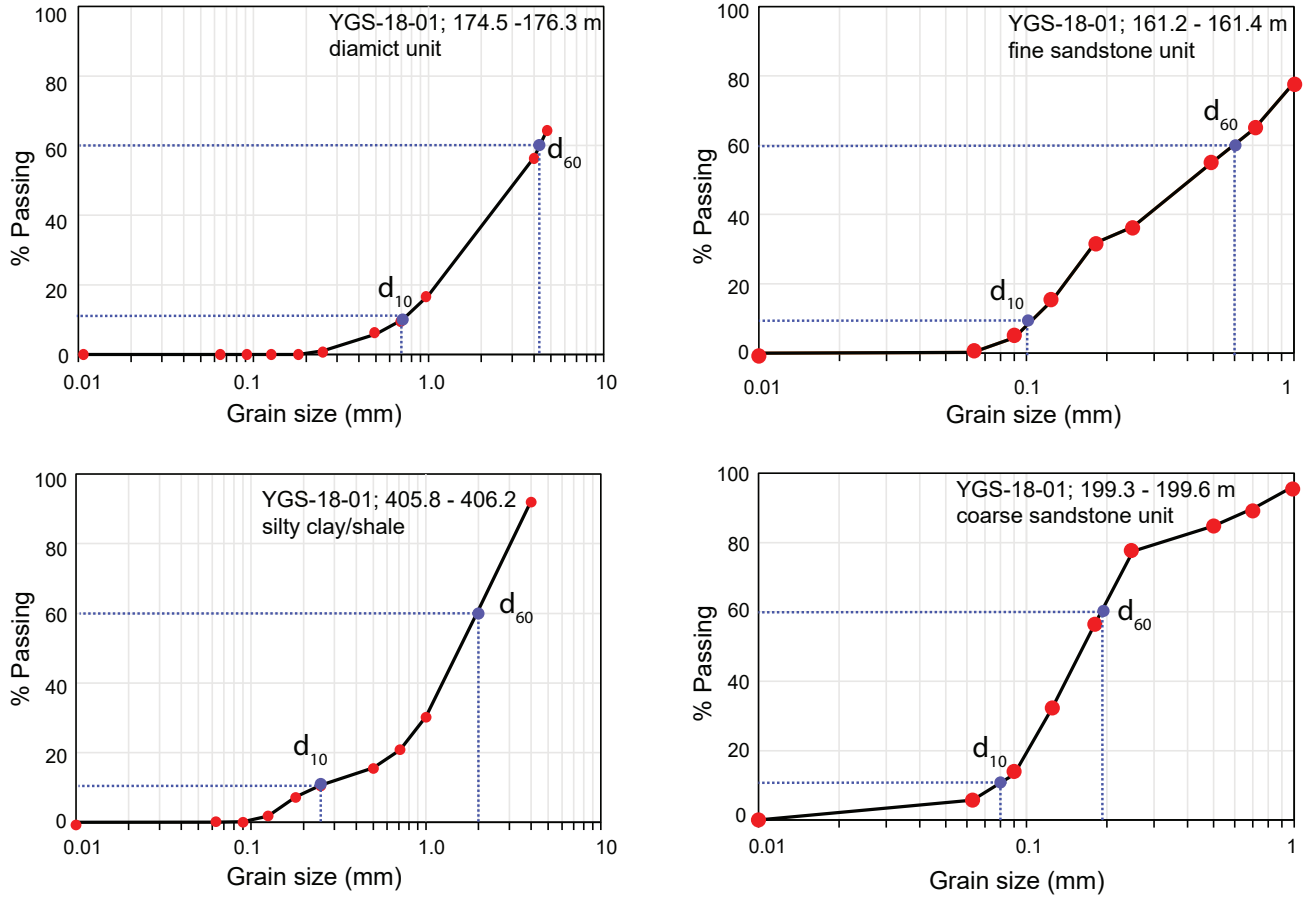

Figure 18. *Grain size distribution of Tintina well (YGS-18-01) rock units.*

Geological cross sections

Conceptual cross sections A-A' and B-B' (Figs. 13 and 19) show the distribution of geological units influencing heat transfer and groundwater flow in the vicinity of the Takhini well. Basement rocks consist of variably deformed and metamorphosed greenstone of the Takhini assemblage. Triassic to Jurassic sedimentary sequences and volcaniclastic strata overlie the Takhini assemblage. Steeply dipping north-trending normal faults separate the sedimentary basin into segments as a result of regional tectonic activity in pre-Late Cretaceous (Hart, 1997). Eocene granitoid plutons intruded Triassic to Jurassic sedimentary sequences and volcaniclastic strata (Hart, 1997). Fault extensions and thickness of rock units at depth are interpretive due to the lack of geophysical or deep well data in this area.

Discussion

Heat transfer and groundwater flow

Takhini well (YGS-17-01)

Heat transfer mechanisms in the Takhini well include both conduction and forced convection. Conduction refers to the process of heat transfer that takes place between materials by direct contact, while convection refers to heat transfer driven by fluid flow. A distinction can be made between auto (natural) convective and forced convective heat transfer. The former occurs in hot and permeable rocks such as in an active volcanic environment where there are significant temperature contrasts in rocks with high hydraulic conductivity. The latter occurs in deep and confined aquifers with significant connectivity over long distance with sufficient hydraulic gradient to induce fluid movements (Sass and Götz, 2012).

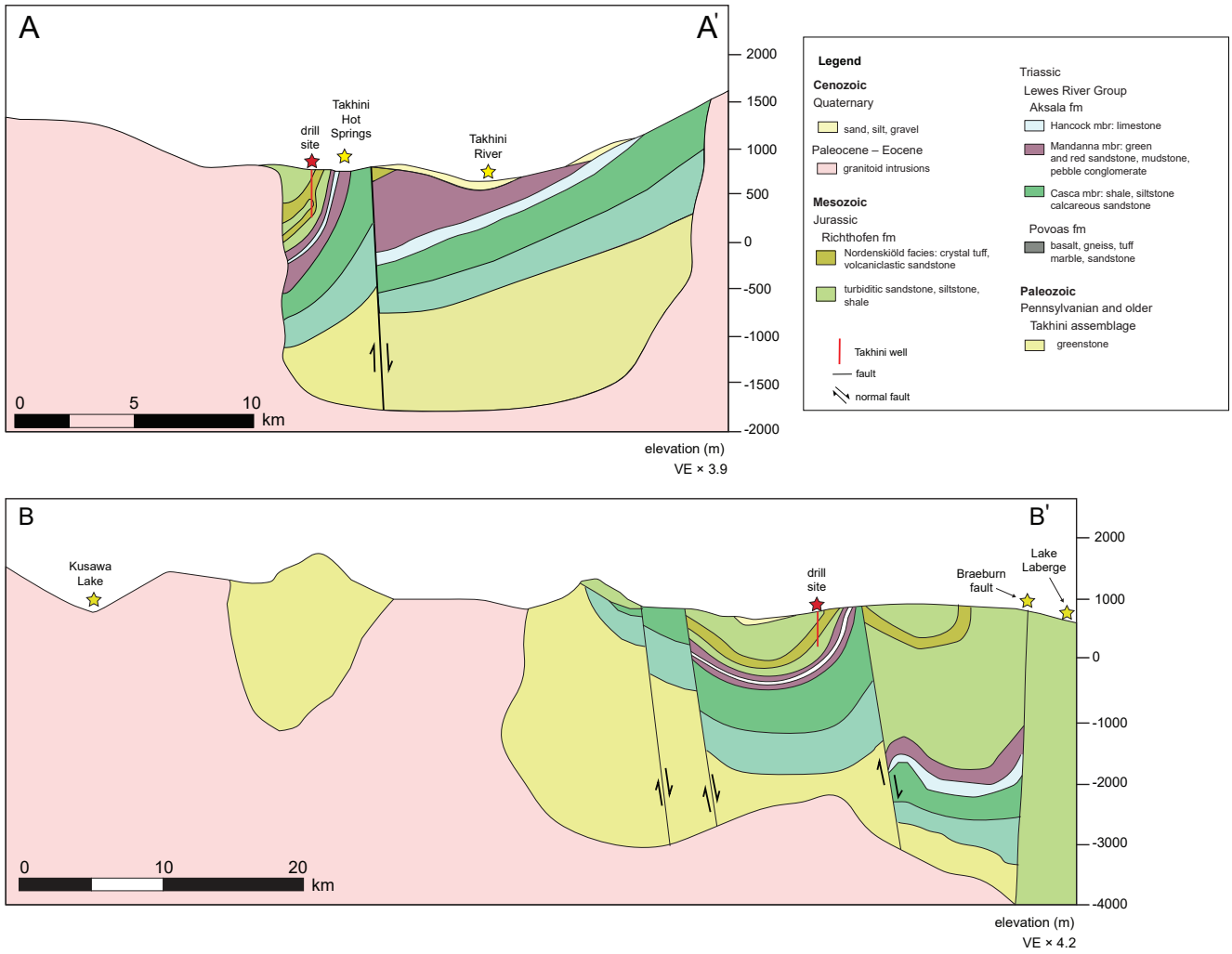

Figure 19. *Schematic geological cross-sections A–A' and B–B' through the Takhini well (YGS-17-01). Location of cross sections are shown in Figure 13. Geology after Hart (1997), Colpron et al. (2015), and Yukon Geological Survey (2018a).*

Temperature measurements and analysis of thermo-hydraulic properties in the Takhini well indicate that conduction is the main mechanism of heat transfer in the well above 450 m. The low thermal conductivity variation between units (Table 1), no drastic change in the geothermal gradient, and a smooth and near-linear temperature profile above 450 m depth (Fig. 2a) are characteristic of heat conduction (Sass and Götz, 2012).

The high geothermal gradient of 250°C km^{-1} observed below 450 m depth shows a drastic change in temperature of ~12.5°C over a depth of 50 m. This heat transfer cannot be explained by conduction as the thermal conductivity is similar for the whole well and surrounding outcrops (generally <9.6 × 10^{-9} m s^{-1}). Instead, the temperature anomaly in the lower part of the well is interpreted as forced-convective heat transfer caused by deep, warmer groundwater rising along fractures. Sass and Götz (2012) suggest that heat transfer in rocks transitions from forced convective to auto (natural) convective over a hydraulic conductivity increase from 10^{-9} m s^{-1} to 10^{-5} m s^{-1} (Fig. 20). The matrix hydraulic conductivity of rock samples in the Takhini well and surrounding outcrops is generally <9.6 × 10^{-9} m s^{-1}, suggesting conductive heat transfer, however, the presence of fractured and unconsolidated rocks may provide a higher hydraulic conductivity to

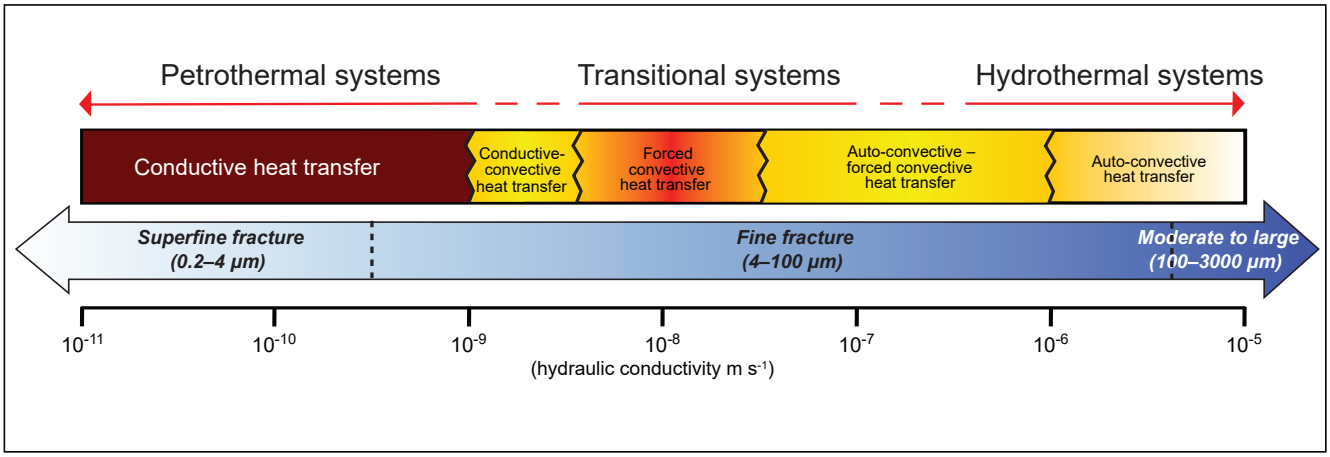

Figure 20. *Classification of geothermal systems based on the dominant mechanism of heat transfer (convective vs. conductive; after Sass and Götz, 2012).*

achieve convective heat transfer. Figure 15 shows that fine to large fracture apertures in the Takhini well can provide adequate hydraulic conductivity (>10^{-9} m s^{-1}) to allow forced convective to auto-convective heat transfer. As auto convection only induces groundwater movement in rocks with significant temperature contrasts and high hydraulic conductivity, forced convection is most likely driving groundwater movement in the Takhini region which is controlled by the regional hydraulic gradient in an aquifer system of moderate hydraulic conductivity. For example, this can occur where topographic highs in a mountain range act as a recharge zone for water that discharges in lower altitude valleys provided there is adequate fracture connectivity in the host rock. As fine and moderate to large fracture apertures and unconsolidated rocks in the Takhini well have a hydraulic conductivity that is mostly greater than 10^{-9} m s^{-1} (Fig. 15), forced convective heat transfer can occur and trigger the formation of a hydrothermal system and hot springs, provided that fractures are interconnected. The Takhini well and the hot springs are located in a topographical trough (Fig. 21), where the difference in elevation (~500 m over ~15 km distance) can cause a strong hydraulic gradient. Data provided from one well is not enough to evaluate fracture connectivity in this study, and it is difficult to correlate any permeable zones observed in the core samples of the Takhini well with the high geothermal gradient at the bottom of this well (>450 m). Despite these limitations, the thermal-hydraulic properties assessed in this study suggest the forced convective heat transfer hypothesis remains the most plausible for the temperature spike in the bottom of the well. Assuming that faults and fractures are interconnected and have hydraulic conductivity at least greater than 10^{-9} m s^{-1}, regional groundwater flow can be directed toward the Takhini River and upflow can occur along faults, creating a resurgence under the Takhini well near the river, a major waterbody collecting groundwater.

Tintina well (YGS-18-01)

Heat transfer and groundwater flow in the Tintina well can be similarly related to the Sass and Götz (2012; Fig. 20) classification of geothermal systems. The low thermal conductivity contrast and linear geothermal gradient are characteristics of conductive heat transfer in the well. Hydraulic conductivity estimations for unconsolidated/brecciated rocks of the Tintina well suggest permeable rocks, with hydraulic conductivity ranging from 10^{-5} to 10^{-3} m s^{-1} (Table 5). These values fall within an auto-convective heat transfer realm, which could trigger the formation of warm hydrothermal systems in the area, however, no hot springs or surface seeps are known.

Geothermal setting

Takhini Hot Springs region

The geological setting in the Takhini area is typical of an orogenic belt, where conductive and forced convective heat transfer can occur (Moeck, 2014). Geological features, such as steeply dipping crustal faults, can favour forced convective heat transfer as they are preferential paths for rising warm groundwater. Figure 22 illustrates schematic isotherms and water flow line interpretations based on the main recharge areas and major faults in the area. Groundwater recharge areas are commonly associated with elevated mountainous regions and the discharge dominantly occurs near the Takhini River. From recharge to discharge, groundwater tends to flow through permeable rocks. Several north-trending steep normal faults cut strata in the Takhini area (Hart, 1997) including one that crosscuts the center of the A–A' cross section (Fig. 21). This major feature can affect the groundwater flow path as it is believed to be more fractured and permeable than rocks outside the fractured zone. Due to the hydraulic head difference between the top and the base of the fracture, deep water heated from the Takhini area's local geothermal gradient can rise along the fault to create shallower isotherms. This can form hot springs like Takhini Hot Springs where well-connected fractures allow a constant groundwater discharge (Fig. 22).

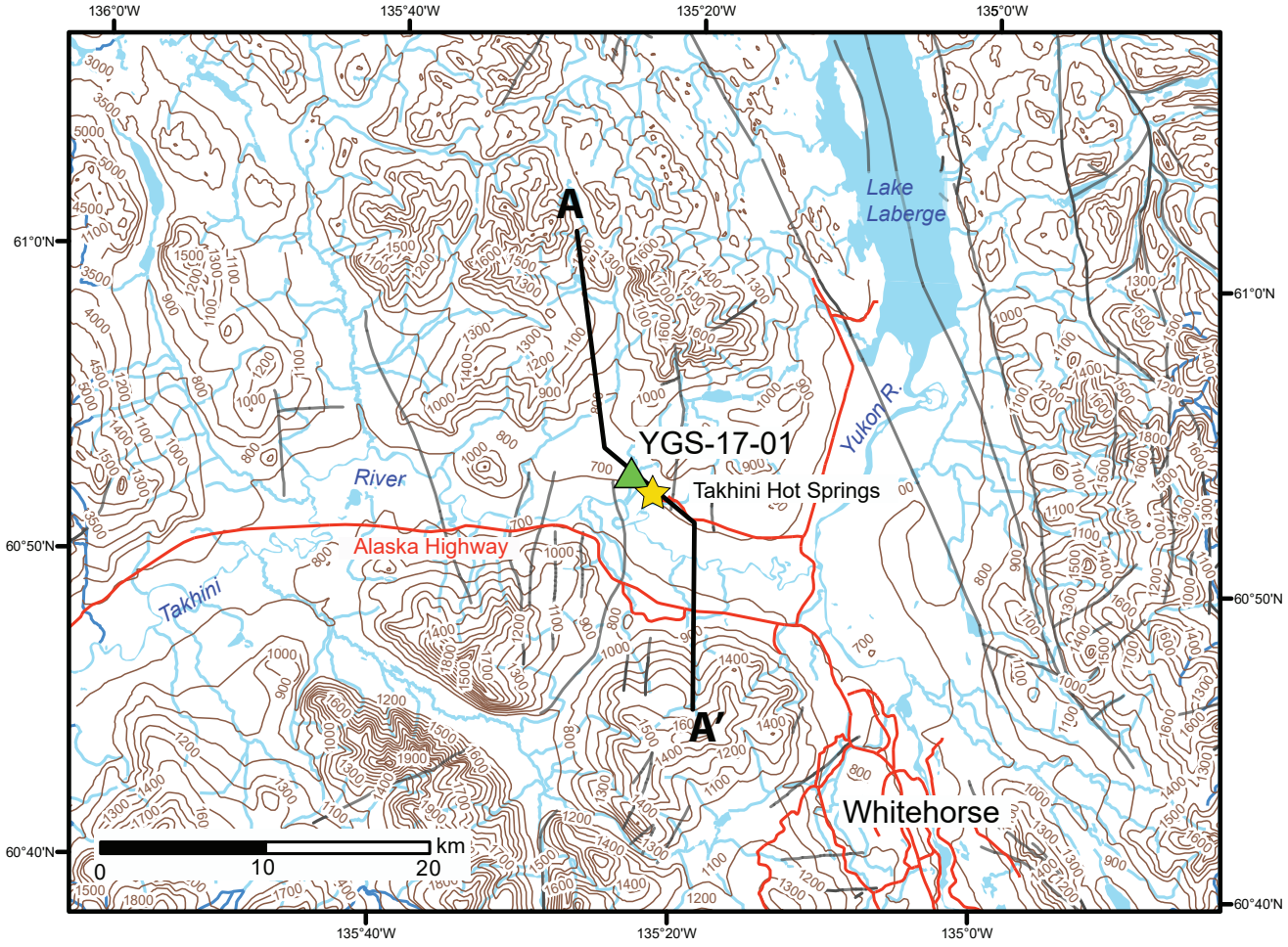

Figure 21. *Topographic map of the Takhini well area, with locations of cross sections (A–A') in Figure 22. Contour intervals in metres. Grey lines denote surface expression of faults (Yukon Geological Survey, 2018a).*

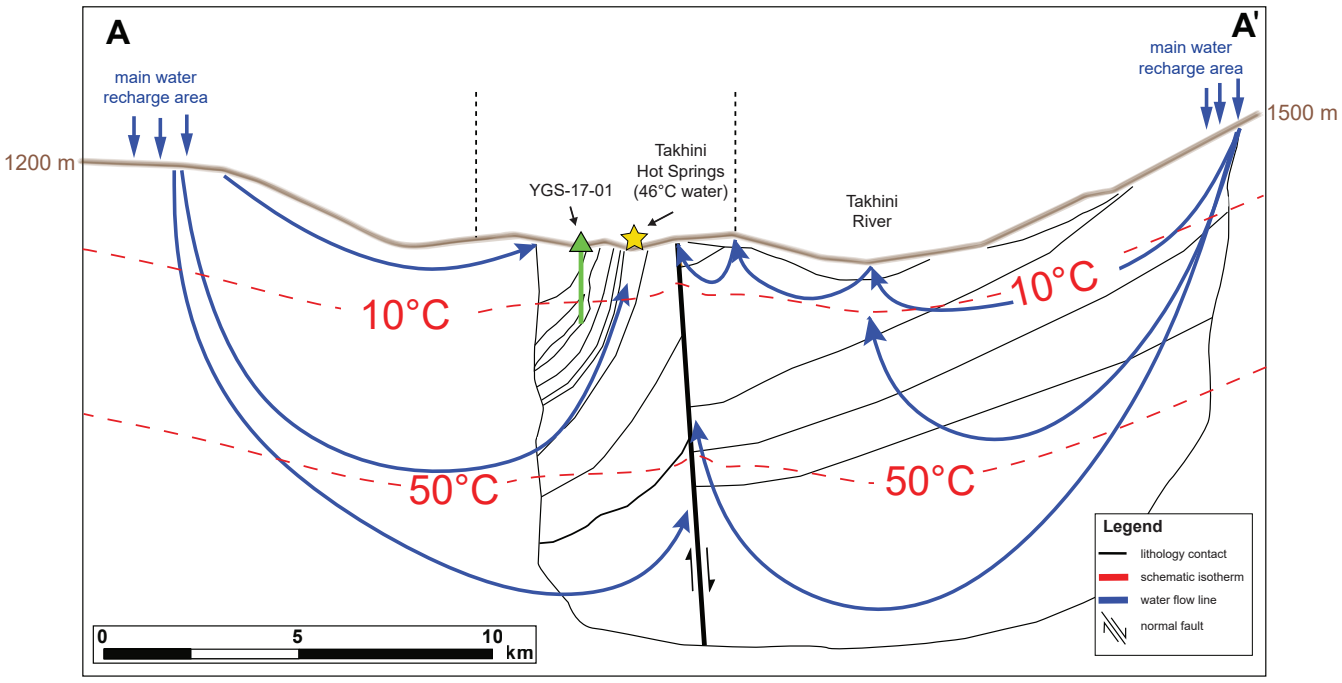

Figure 22. *Conceptual hydrothermal system of the Takhini Hot Springs area according to geothermal play-types in orogenic belts; after Moeck (2014). Vertical axis is schematic and depth of isotherms approximated. Dotted vertical lines indicate where cross section line changes direction.*

Tintina well region

The Tintina well has a different hydrogeological setting compared to the Takhini well. Regional groundwater flow near the Tintina well is more likely to come from a shallow aquifer due to the proximity of high mountains (Figs. 23 and 24), explaining why the observed temperature profile does not appear to be affected by upwelling warm water even though the rocks are fractured and appear to be permeable. Groundwater can rise along major faults if there is a significant hydraulic head difference between the base and the top of faults, commonly caused by fault orientation and topography with recharge at mountain highs and discharge in valleys. Such regional groundwater flow can exist in the Tintina Trench area where the main waterbody collector is the Pelly River. However, the hydraulic head difference along the faults may not be enough for the deep groundwater to rise since the Tintina fault is likely to be subvertical (Welford *et al.*, 2001) and hydraulic head is expected to remain similar along this major fault. Therefore, the discharge area is mainly sourced by the cold water from the mountain highs. The geological setting in the Tintina Trench is typical of an orogenic belt, but the hydrogeological context is not favourable for hot spring development.

Conclusions

This study has defined the thermo-hydraulic properties of rocks in, and within, the vicinity of the Takhini temperature gradient well (YGS-17-01) and in the Tintina well (YGS-18-01), in southern Yukon. The new data, combined with the temperature gradient measured in the wells, offers explanations for heat transfer mechanisms. In addition, hydrothermal conceptual models of the well locations are presented. The thermal conductivity results show that conductive heat transfer dominates the Takhini well to a depth of 450 m, as the temperature profile is near-linear and thermal

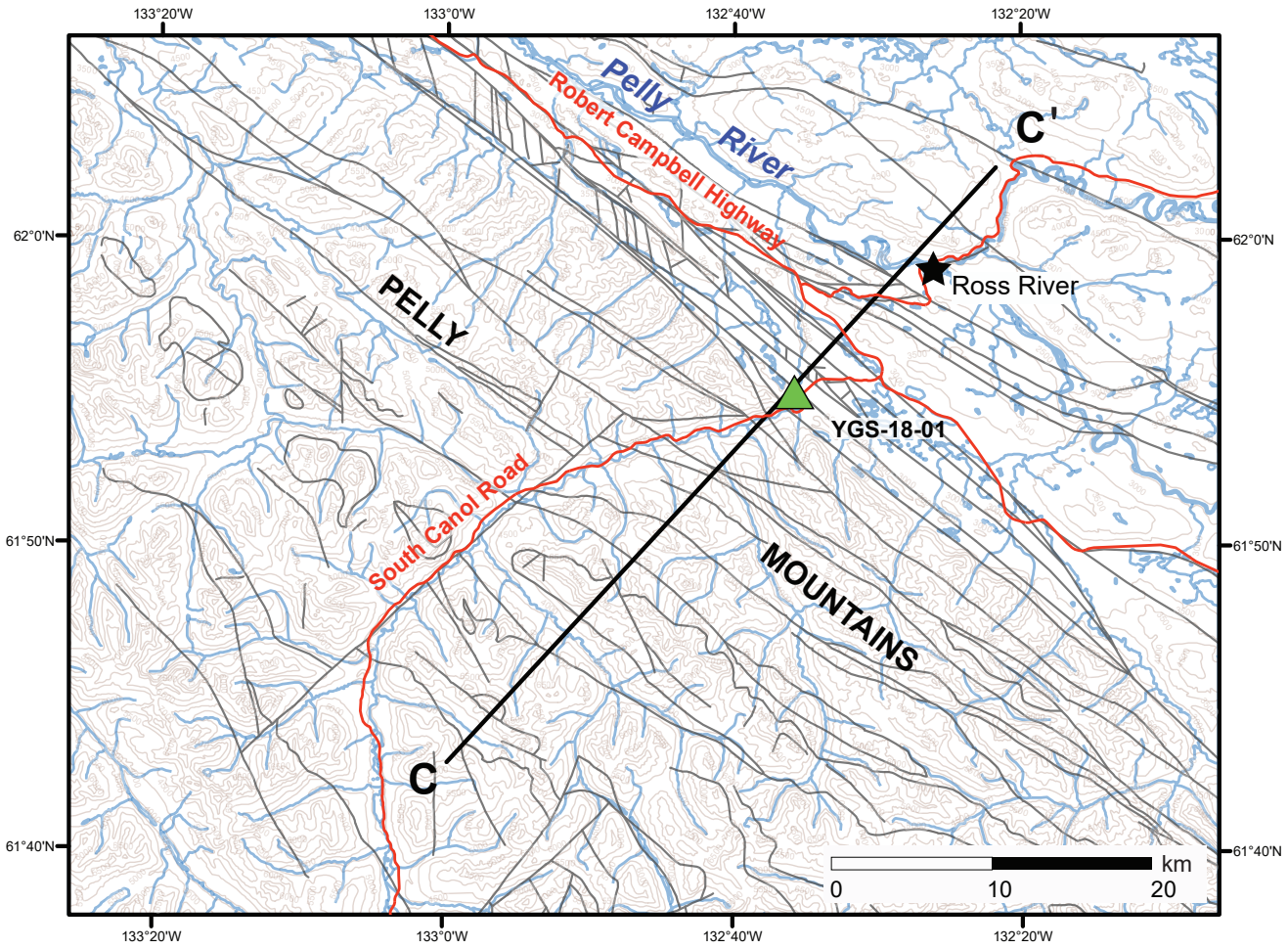

Figure 23. *Topographic map of the Tintina trench well area with the location of cross section C–C' in Figure 24. Contour intervals in feet. Grey lines denote surface expression of faults (Yukon Geological Survey, 2018a).*

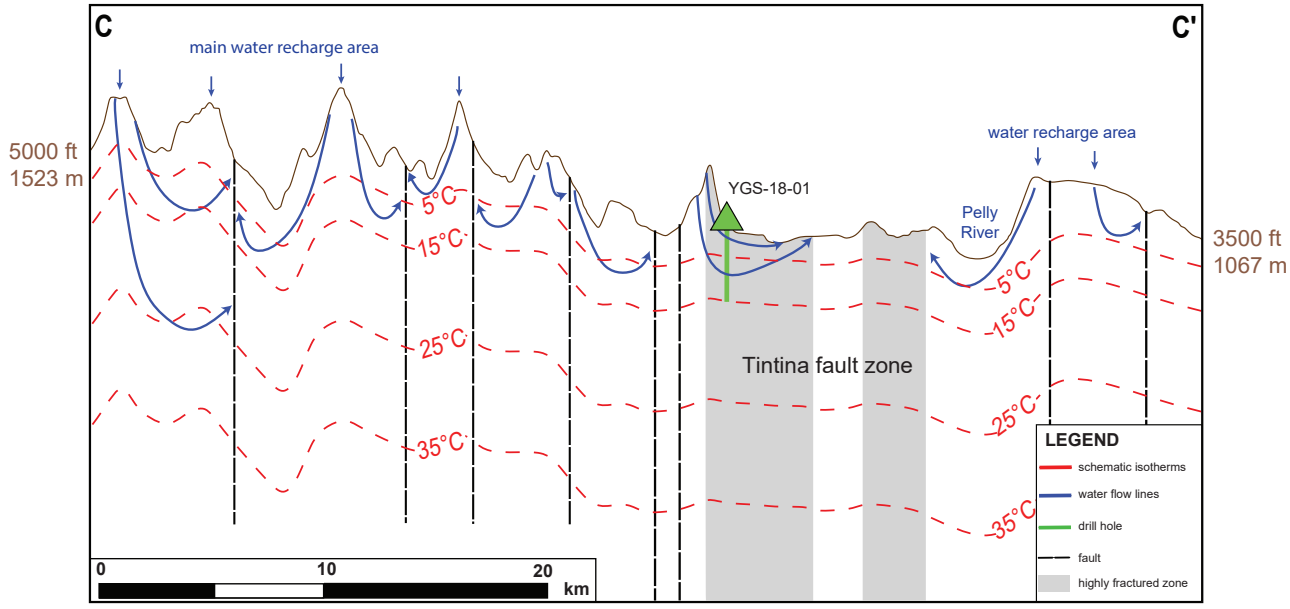

Figure 24. *Conceptual hydrothermal system of the Tintina well area according to geothermal play-types in orogenic belts; after Moeck, (2014). Vertical axis schematic and depth of isotherms approximated. Not all faults are indicated on the cross section which are on the map, for model simplicity.*

conductivity contrasts between lithological units are minor. The elevated geothermal gradient observed at the bottom of the Takhini well (250°C km^{-1}) and the thermal manifestations at Takhini Hot Springs are likely caused by forced convective heat transfer associated with deep groundwater flow in permeable fractures generating a hydrothermal system typical of a geothermal play type in an orogenic belt (Fig. 22). The ~2 km lateral distance between warm water at the bottom of the Takhini well and the Takhini Hot Springs can give an approximate estimate of the extent of this warm fluid ascending zone, assuming there is interconnectivity of fractures. This study did not identify the heat source for the hot water at Takhini, however, this would be a good future study, specifically a focussed evaluation of the distribution and radioactive heat potential of igneous intrusions in the vicinity to evaluate their role in the geothermal system.

Thermo-hydraulic properties of rocks in the Tintina well, including little thermal conductivity contrasts between rock units and a linear geothermal gradient, suggest that conductive heat transfer dominates the well, and groundwater in the well is likely sourced from shallow aquifers. Unlike the Takhini setting, no hot springs or seeps are known from this area.

Assessment of the thermal conductivity can be used with calculated radiogenic heat production values from geological units in the region as a next step to evaluate heat flow and extrapolate temperature at depth. Quantifying the natural amount of heat originating from the Earth's interior and based on Fourier's Law, the heat flux density is needed to define boundary conditions of numerical groundwater flow and heat transfer models to quantitatively confirm the heat transfer hypotheses formulated in this work. Such an approach would be helpful to improve understanding of the origin of the Takhini Hot Springs. Such a model can be used to reproduce the temperature measured in the Takhini well or at the hot springs to better explain the factors controlling the formation of the hydrothermal system.

The geological context of Yukon shows potential for geothermal energy with many hot springs like Takhini. Geothermal exploration done by the YGS provides more data to evaluate this potential around the hot springs. Further calculations and simulations combined with the measurements obtained with this study will bring a better comprehension of resources to move towards an evaluation of the likelihood of geothermal energy resources in this region.

Acknowledgements

The Takhini well (YGS-17-01) was drilled on Category A land of the Ta'an Kwäch'än Council – we are grateful for their collaboration on this project, and for providing access to outcrops in summer 2019. The Tintina well was drilled in the traditional territory of the Liard First Nation, in partnership with the Ross River Dena Council. We are grateful for the opportunity to collaborate with these First Nations on these important ground temperature studies. This work was funded by a Discovery grant from the Natural Sciences and Engineering Research Council of Canada awarded to INRS and a scholarship from the Armand-Frappier Foundation awarded to the first author. Maurice Colpron (YGS) provided field, technical, and GIS guidance for which we are appreciative. Liam Maw is acknowledged for thin section descriptions and Bailey Staffen (YGS) for GIS assistance. Carolyn Relf (YGS) is acknowledged for ongoing managerial and funding support of student geoscience projects.

References

Alvarado Blohm F.J., 2016. Determination of hydraulic conductivities through grain-size analysis. MSc thesis, Boston College University Libraries, Chestnut Hill, United States, 102 p.

Beyer, W. 1966. Hydrogeological investigations in the deposition of water pollutants. Journal of Applied Geology, vol. 12, p. 599–606.

Bordet, E., Crowley, J.L. and Piercey, S.J., 2019. Geology of the eastern Lake Laberge area (105E), south-central Yukon. Yukon Geological Survey, Open File 2019-1, 120 p.

Colpron, M., Israel, S. and Friend, M., 2016. Yukon plutonic suites. Yukon Geological Survey, Open File 2016-37, scale 1:750 000.

Colpron, M., Crowley, J.L., Gehrels, G.E., Long, D.G.F., Murphy, D.C., Beranek, L.P. and Bickerton, L., 2015. Birth of the northern Cordilleran orogen, as recorded by detrital zircons in Jurassic synorogenic strata and regional exhumation in Yukon. Lithosphere, vol. 7, p. 541–562.

Core Lab Instruments, 2016. PPP-250 Portable probe permeameter operations manual. Core Lab Instruments. Tulsa, United States, p. 6.

Decagon Devices Inc., 2012. KD2 Pro Thermal properties analyser: operator's manual, version 12. Decagon Devices Inc. Pullman, United States, 68 p.

Duggal, K.N. and Soni, J.P., 1996. Elements of Water Resources Engineering. New Age International (P) Limited, p. 270.

Fraser, T.A., Grasby, S.E., Witter, J.B., Colpron, M., Relf, C., 2018. Geothermal studies in Yukon-collaborative efforts to understand ground temperature in Canadian North. GRC Transactions, vol. 42, 20 p.

Friend, M., and Colpron, M., 2017. Potential radiogenic heat production from Cretaceous and younger granitoid plutons in southern Yukon. Yukon Geological Survey, Open File 2017-60, scale 1:1 000 000.

Gabrielse, H., Murphy, D.C. and Mortensen, J.K. Cretaceous and Cenozoic dextral orogeny parallel displacements, magmatism and paleogeography, north-central Canadian Cordillera. *In:* Paleogeography of the North American Cordillera: Evidence For and Against Large-Scale Displacements, Haggart, J.W., Monger, J.W.H. and Enkin, R.J. (eds.). Geological Association of Canada, Special Paper 46, p. 255–276.

Hart, C.J.R., 1997. A transect across northern Stikinia: Geology of the northern Whitehorse map area, southern Yukon Territory (105D/13-16). Yukon Geological Survey, Bulletin 8, 112 p.

Langevin, H., Raymond, J., Comeau, F.-A., Malo, M. and Molson, J., 2019. Évaluation des ressources géothermiques des Îles-de-la-Madeleine. Conférence: XIVème Colloque International Franco-Québécois en énergie, Baie St-Paul, Canada, p. 6.

Langevin, H., Fraser, T. and Raymond J., 2020. Assessment of thermo-hydraulic properties of rock samples near Takhini Hot Springs, Yukon. *In:* Yukon Exploration and Geology 2019, K.E. MacFarlane (ed.), Yukon Geological Survey, p. 57–73.

Lasercomp-TA Instruments, 2020. FOX 50. https://www.tainstruments.com/fox-50/.

Long, D.G.F., 2015. Depositional and tectonic framework of braided and meandering gravel-bed river deposits and associated coal deposits in active intermontane basins: The Upper Jurassic to mid-Cretaceous Tantalus Formation, Whitehorse trough, Yukon, Canada. Yukon Geological Survey, Open File 2015-23, 80 p.

Mira Geoscience, 2017. Ross River geothermal exploration project: Review of the 2014 work program. Miscellaneous Report, MR 18, Yukon Geological Survey, 141 p.

Moeck, I.S., 2014. Catalog of geothermal play types based on geologic controls. Renewable and suitable energy reviews 37, Elsevier, p. 867–882, https://doi.org/10.1016/j.rser.2014.05.032.

Nelson, J.L., Colpron, M., Israel, S, 2013. Cordillera of British Columbia, Yukon, and Alaska: Tectonics and Metallogeny. Society of Economic Geologists Special Publication no. 17, p. 53–109.

Popov, Y.A, Berezin, V.V. and Seminov, V.G., 1985. Evaluating the thermal conductivity of anisotropic minerals and rocks. Izvestiya, Physics of the Solid Earth, vol. 7, p. 565–570.

Popov, Y., Lippmann, E. and Rauen A., 2020. Thermal Conductivity (TC) and Thermal Diffusivity (TD) Scanner-Manual version 9.3.2020, 62 p., http://www.geophysik-dr-rauen.de/tcscan/downloads/TCS-Manual.pdf.

Rybach, L., 1981. Geothermal systems, conductive heat flow, geothermal anomalies. *In:* Geothermal systems: principles and case histories, L.J.P. Muffler and L. Rybach (eds), John Wiley & Sons, New York, p. 3–36.

Sass, J.H., Lachenbruch, A.H., Moses Jr., T.H., and Morgan, P., 1992. Heat flow from a scientific research well at Cajon Pass, California. Journal of Geophysical Research, vol. 97, p. 5017–5030, https://doi.org/10.1029/91JB01504.

Sass, I. and Götz, A.E., 2012. Geothermal reservoir characterization: a thermofacies concept. Terra Nova, vol. 24, p. 142–147, https://doi.org/10.1111/j.1365-3121.2011.01048.x.

Vosteen, H.-D. and Schellschmidt, R., 2003. Influence of temperature on thermal conductivity, thermal capacity and thermal diffusivity for different type of rocks. Physics and Chemistry of the Earth, vol. 28, p. 499–509.

Witherspoon, P.A., Wang, J.S.Y., Iwai, K. and Gale, J.E., 1979. Validity of Cubic law for fluid flow in a deformable rock fracture. Department of Materials Science and Mineral Engineering, and Lawrence Berkeley Laboratory, University of California, Berkeley, 28 p.

Welford, J.K., Clowes, R.M., Ellis, R.M., Spence, G.D., Asudeh, I. and Hajnal, Z., 2001. Lithospheric structure across the craton-Cordilleran transition of northeastern British Columbia. Canadian Journal of Earth sciences, vol.38. p. 1169–1189, https://doi.org/10.1139/cjes-38-9-1169.

Witter, J.B. and Miller, C., 2017. Curie point depth mapping in Yukon. Yukon Geological Survey, Open File 2017-3, 38 p.

Yukon Geological Survey, 2018a. Bedrock geology data set. Compilation. Yukon Geological Survey, http://data.geology.gov.yk.ca/Compilation/3.

Yukon Geological Survey, 2018b. Surficial geology data set. Compilation. Yukon Geological Survey, http://data.geology.gov.yk.ca/Compilation/33.

Appendices

Appendices are only available as digital files. They are included in a .zip file that accompanies this document and available from https://data.geology.gov.yk.ca.

Appendix A. (1) Thermal conductivity scanner measurements for consolidated rocks using a Lippman and Rauen thermal conductivity scanner (TCScan; Popov et al., 2020). **(2)** Thermal conductivity heat flow meter measurements for consolidated outcrop rocks with the FOX50 (Lasercomp-TA Instruments, 2020). **(3)** Thermal conductivity needle probe measurements for unconsolidated rocks with the K2D Pro needle probe (Decagon Devices Inc., 2012)

Appendix B. (1) Whole rock geochemical data (ALS labs). **(2)** Radiogenic heat production calculations (Rybach, 1981).

Appendix C. (1) Hydraulic conductivity measurements for consolidated rocks using a transient gas permeameter (PPP-250; Core Lab Instruments, 2016). **(2)** Hydraulic conductivity measurements for unconsolidated rocks from the grain size distribution (Beyer, 1966). **(3)** Hydraulic conductivity calculations for fractured rocks using the Cubic law (Whiterspoon et al., 1979).